LIÈGE université Library

https://lib.uliege.be

https://matheo.uliege.be

Research master thesis: Study of the isotope effect on the competition between H and H2 loss in ethylene cation using semi-classical molecular dynamics

Auteur : p257459
Promoteur(s) : Remacle, Françoise
Faculté : Faculté des Sciences
Diplôme : Master en sciences chimiques, à finalité approfondie
Année académique : 2022-2023
URI/URL : http://hdl.handle.net/2268.2/17951

Avertissement à l'attention des usagers :

Tous les documents placés en accès ouvert sur le site le site MatheO sont protégés par le droit d'auteur. Conformément aux principes énoncés par la "Budapest Open Access Initiative"(BOAI, 2002), l'utilisateur du site peut lire, télécharger, copier, transmettre, imprimer, chercher ou faire un lien vers le texte intégral de ces documents, les disséquer pour les indexer, s'en servir de données pour un logiciel, ou s'en servir à toute autre fin légale (ou prévue par la réglementation relative au droit d'auteur). Toute utilisation du document à des fins commerciales est strictement interdite.

Par ailleurs, l'utilisateur s'engage à respecter les droits moraux de l'auteur, principalement le droit à l'intégrité de l'oeuvre et le droit de paternité et ce dans toute utilisation que l'utilisateur entreprend. Ainsi, à titre d'exemple, lorsqu'il reproduira un document par extrait ou dans son intégralité, l'utilisateur citera de manière complète les sources telles que mentionnées ci-dessus. Toute utilisation non explicitement autorisée ci-avant (telle que par exemple, la modification du document ou son résumé) nécessite l'autorisation préalable et expresse des auteurs ou de leurs ayants droit.

FACULTE DES SCIENCES
Chemistry Department

Theoretical Physical Chemistry – Françoise Remacle

Study of the isotope effect on the competition between H and H_2 loss in ethylene cation using semi-classical molecular dynamics

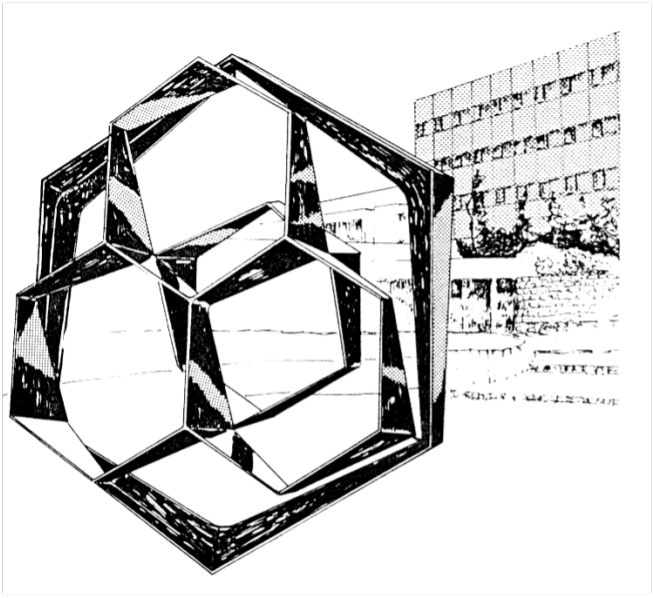

Academic year 2022-2023

Written by Julie HAMMOUD
To obtain the master's degree in Chemistry

Acknowledgments

Firstly, I would like to thank Prof. Françoise Remacle for allowing me to do my master thesis in her research group. I would like to thank her for always taking the time to explain quantum dynamics concepts to me and to push me to give my best throughout this master thesis.

Many thanks to Manuel who helped me a lot to handle the computational aspects of my thesis, and who always was there to answer my questions. Working with him on this project was extremely motivating.

Thanks a lot, to my colleagues Shouryo, James and Gaurav who gave me new inputs and perspectives that made me clarify my mind on my subject.

I would like also to thank the FAME+ master consortium for allowing me to be part of this Erasmus Mundus degree program. They gave me the opportunity to study in two well-known European universities. Being enrolled in this program was also enriching on a personal point of view, it allowed me to meet people from all around the world and opened my mind to new cultures and languages.

Finally, I am very grateful to the people around me including my family, Christoph and Camille who were always there for me as a mental support. Their curiosity on my subject helped me to capture its main idea and express it in a simple way.

Abstract

The engineering of atto second and short femtosecond pulses opened the way to probe ultrafast dynamics during the past 20 years. Being able to follow a mechanism on a sub or few femtoseconds time scale allowed scientists to investigate reaction mechanisms that were still not fully understood. The dissociation of ethylene cation is a multipathway reaction leading to either H loss or H_2 loss. Substituting the hydrogen atoms by deuterium provides further understanding on the relaxation and reaction mechanisms and on the competition between the two pathways. The relaxation dynamics of the four lowest electronic states of C_2D_4+ were computed semi-classically using the Surface Hopping including Arbitrary Couplings (SHARC) software for the first few dozens of fs. After relaxation to the ground state, the longer, picosecond, dynamics was computed using classical Born-Oppenheimer molecular dynamics (BOMD). The relaxation from excited electronic states to the ground state of the cation is ultrafast and occurs during the first 50 fs. Our results demonstrated that the isotope substitution impacts the relaxation dynamics from the excited states. The process is slower due to the mass difference between hydrogen and deuterium. The type of conical intersection visited by the molecule during its relaxation is also impacted by the isotope effect. We compared our results to experimental results for deuterated ethylene cation as well to those obtained for the hydrogenated ethylene in a previous study. We further analyzed the steps of the mechanism for D loss and D_2 loss including transition states and intermediates and compared our results to those available in the literature.

Table of contents

Introduction

Chemistry is the science of transformation of matter. At the molecular scale, it involves the modification of the geometry of molecules to go from reactants to products meaning that a rearrangement of the chemical bonds is occurring. Some bonds in the reactants are broken, new bonds are formed in the products [1]. The concept of a 'bond' means a localization of the electronic density between two nuclei that decreases the Coulomb repulsion between them so that a stable molecule is formed. A chemical reaction, going from reactants to products, therefore implies a change of the localization of the electronic density between the nuclei.
If one wants to understand the chemical reaction, one therefore needs to be able to probe the electronic motion that accompanies to nuclei rearrangements as well as the motions of the nuclei themselves [1].
The theory of quantum mechanics of Schrödinger (1925) [2] contributed to understand more precisely the interactions between atoms. The time dependent Schrödinger equation describes the evolution of a system over time and is the fundamental equation of quantum mechanics. The time independent Schrödinger provided a way to calculate the electron density probability for a given electronic state and led to the Born-Oppenheimer approximation (BOA) and to the concept of potential energy surface (1927) [1,2].
Nevertheless, solving the time-independent Schrödinger equation exactly is not possible for molecules. [1] To solve this equation, one relies on the Born-Oppenheimer approximation (1927) [1] (BOA) based on the mass difference between the nuclei and electrons. The electrons being 2 000 lighter than the nuclei, their motion is faster. The electronic motion is occurring at the attosecond time scale (10^{-18} second to few femtoseconds (1 fs = 10^{-15} s)). On the other hand, the nuclei are moving on a slower femtosecond to picosecond (10^{-12} seconds) time scale. Consequently, the total wave function describing the nuclei and the electrons can be separated into two wave functions, one for the nuclei and one for the electrons. This is an adiabatic approximation where the nuclei and electrons are treated independently [1].

The solutions of the time-independent Schrödinger equation provide potential energy surfaces for the motion of the nuclei which can be used to solve the time dependent Schrödinger equation. It is however also not possible to solve exactly the time-dependent Schrödinger equation for nuclei because of the large number of molecular degrees of freedom. One can then make the approximation that the nuclei move according to the laws of classical mechanics and solve the Newton equations of motion [2].

The methodologies developed during the XX century to compute molecular dynamics contributed to understand better how the electrons and nuclei were interacting with each other and how to model chemical reactivity at the atomic and molecular scale. The challenge for experiments was to capture bond rearrangements from reactants to products over time. The motion of the nuclei is in the femtosecond to picosecond range so at 10^{-15} to 10^{-12} seconds. Around the 90s, no experimental set-up was precise enough to capture this motion in real time [3,4].

In 1999, Prof. Ahmed H. Zewail received the Nobel prize of chemistry for his work in ultrafast dynamics for developing a laser technology that allowed to produce laser pulses of a duration of 20 – 100 fs, that were short enough to capture the evolution of the nuclei during a chemical reaction [5].

The experimental approach developed by A. H. Zewail is using femto-second laser pulses in a pump-probe scheme. The reactants are excited to higher electronic states with a laser pulse which takes the nuclei out of equilibrium, this is the “pump”. Then a delayed second laser pulse will “probe” the time evolution of the excited molecule, it will scan it or “take a picture”. By varying the time between the “pump” and the “probe” steps, it is then possible to probe the reaction path and to identify possible transition states or intermediates during the reaction. This revolution in photochemistry provided a detailed analysis of a reaction over time and allowed to characterize intermediate steps before obtaining the final product [5].

Few years later, an optical pulse even shorter was developed allowing to capture motion in the attosecond range (10^{-18} second) which corresponds to the time scale of the motion of the electrons. This attosecond pulse is produced with High-Order Harmonic Generation. Generating a harmonic can be explain semi-classically with three main steps [6]. First, a femtosecond laser pulse applied on a gas target (usually rare gas atoms) will distort the potential well of the atoms. Consequently, an electron will tunnel away from the nucleus. This first step is called the “tunnel ionization”. Once the electron is not in the potential well anymore, it will move freely and is accelerated by the electric field applied. This is the “motion after ionization” step. Finally, when the electric field will change sign, the electron is decelerated and will go back to its initial position in the potential well. This “recollision” step with the nucleus also involves the emission of a photon in the extreme-ultraviolet range (10 to 120 nm). This photon, depending on the initial wavelength of the laser and the intensity of the electric field, will have an energy that can reach hundreds eV. Depending on what we want to investigate, the energy of the photon required will not be the same [3]. If we want to excite the electrons localized on the valence orbitals for a medium size polyatomic molecule, the photon energy must be around 3 to 5-6 eV. But if we want to excite the core electrons, the energy of the photon must be larger, around 200-300 eV.

The engineering of atto pulses led to a new photochemistry field: attochemistry which focuses on ultrafast reaction mechanisms driven by electrons [3]. On the long term, the ability to directly address electrons in molecules but also in solids opens the way to new applications in the field of drug design, medical imaging, faster computers [7].

Attopulses are a new tool in photochemistry to probe ultrafast reaction mechanisms. One well-known example is the photodissociation of the ethylene cation that will be studied in this thesis. With excitation energies up to around ≈ 3-6 eV, the ethylene cation can dissociate in two distinct ways leading to either H or H_2 loss. When the cation is ionized to excited electronic states, the relaxation to the ground state is ultrafast and occurs within the first dozen of fs. Then, the fragmentation occurs on the ground state of the cation on a much longer, hundreds of fs to ps, time scale. Depending on the fragmentation that will occur, different mechanisms with different transition states are involved. Short femto and atto pulses are therefore indispensable to be able to probe the relaxation to the ground state and analyze these mechanisms. Experimentally, it was found that there is a correlation between the initial excitation of the molecule to specific electronic states and the relative fragmentation yields [8,9,10,11,12].

However, these experimental results must be completed with computational simulations in order to get more information about the relaxation and reaction mechanisms and the competition between the two fragmentation pathways.

Quantum dynamics is based on solving the time-dependent Schrödinger equation which describes the evolution of system over time. As discussed above, this equation is not solvable for systems of more than 3-4 nuclei due to a too large number of degrees of freedom. Also, the larger a molecule is, the higher will be the computational cost [13]. By using the approximations presented above, so the Born-Oppenheimer approximation for defining potential energy surfaces for the motion of the nuclei and the classical treatment of the nuclei motion, it is possible to describe approximately the dynamics of large systems in full dimensionality on the nuclear motion. The Born-Oppenheimer approximation is valid if just one electronic state is considered during the simulation, which implies that this electronic state does not get close in energy to other ones [1]. When electronic states are close in energy or crossing each other, the BOA is not valid anymore due to the coupling between the nuclei and the electrons. Conical intersection are regions where two potential energy surfaces are close and so regions where the BOA breaks down [1]. A non-adiabatic coupling is occurring meaning that the electrons and nuclei cannot be treated separately. As the two PES are close in energy, the system can go to another electronic state without absorbing or emitting a photon: it is a radiationless transition. This type of coupling is very common in photochemistry where the molecule is typically promoted to an excited electronic state with light. In the experiments on the photodissociation of the ethylene cation that we simulate in this thesis, several electronic states coupled by non-adiabatic interactions are involved, meaning that we will need to deal with conical intersections [1] to describe the dynamics.

Surface Hopping is a semi-classical computational method that can approximate non adiabatic transitions between electronic states. An ensemble of classical trajectories is used to simulate the motion of a quantum wave-packet from a potential energy surface to another one. Here, for each trajectory, the nuclei are moving classically on the PES defined by the electronic state in an adiabatic way. When the system gets close to a conical intersection, the system can *hop* from a PES to another. This method is widely used to model quantum phenomenon using classical mechanics. The advantage is that the classical motion of the nuclei can be computed "on the fly" for all the nuclear degrees of freedom meaning that the potential energy surfaces do not need to be precomputed before the simulation [2].

During this master thesis, we investigated the relaxation and reaction dynamics of the deuterated ethylene cation, $C_2D_4^+$. The Surface Hopping including Arbitrary Couplings (SHARC) software and Born-Oppenheimer molecular dynamics (BOMD) were used to compute the dynamics. The results of the dynamical simulations were compared to the experimental results obtained by M. Lucchini, et al. [14] The relaxation of the hydrogenated ethylene cation, $C_2H_4^+$, was previously studied [8], the interest of replacing the hydrogen atoms by deuterium is to investigate the isotope effect on the dynamics. In fact, using this isotope which is twice heavier than the hydrogen will influence the rate of the motion of the nuclei on the PES. As a consequence, every characteristic depending on the mass of the nuclei will be impacted (frequencies of the normal modes, dynamical relaxation time …).

This thesis is divided in four main parts. The first chapter is dedicated to the description of general concepts of molecular dynamics. In the second chapter, we summarize the previous study made by M. Lucchini, B. Mignolet et al. [8] about relaxation and reaction dynamics of hydrogenated ethylene cation. Both experimental and theoretical results are presented as well as the experimental results of the relaxation dynamics of deuterated ethylene cation (unpublished, private communication). The methodology used to simulate the dynamics of $C_2D_4^+$ is presented in the third chapter. In the last chapter, we report and analyze the results of the simulations and compare them to the previous experimental results for $C_2H_4^+$ and to the experimental results for $C_2D_4^+$. Finally, the conclusion will summarize the important points of this study and a perspective for future work.

1. Molecular dynamics

Chemistry is a natural science that investigates composition, properties and behavior of matter. This science is implemented in a lot of fields from our everyday life like pharmacology (how a medicament is absorbed in the human body), environmental science (analysis of the ocean composition to determine the impact of global warming on Earth), materials science (investigation on the microstructure of a material) … [15]
Coming back to the fundaments of chemistry, it is crucial to understand how a system, so combination of nuclei and electrons, are interacting over time to evolve from reactants to products. Quantum molecular dynamics is a theorical approach for investigating the quantum evolution of molecular systems over time [1].

1.1 The Schrödinger equation

The time-dependent Schrödinger equation (TDSE) is the fundamental equation of quantum dynamics [2]:

$$\widehat{H}\,\psi(r,R,t) = i\hbar\frac{\partial\psi(r,R,t)}{\partial t} \quad Eq.1.1$$

Where $\widehat{H}$ is the molecular Hamiltonian, $\psi(r,R,t)$ is the wave function of the system depending on the electronic coordinates r, nuclear coordinates R and time t.
The number of internal degrees of freedom of a non-linear molecule is equal to 3N-6 where N is the number of atoms. Regarding these degrees of freedom, the bigger the molecule is, the larger the number of the degrees of freedom will be. Therefore, solving numerically the time dependent-Schrödinger equation for large molecules is complex due to the multidimensionality of the wave-functions [1]. Solving numerically the TDSE in full dimensionality for large molecules is not computationally feasible. Going beyond 3-4 nuclear degrees of freedom and a dozen of electronic states is very expensive on a computational point of view [13].

When the Hamiltonian does not depend explicitly on time, the time-dependence of the eigen wave functions is a trivial phase factor given by the eigenvalues of the stationary Schrödinger equation also called the time-independent Schrödinger equation, expressed as follow [1]:

$$\widehat{H}\,(r,R)\,\psi_n(r,R) = E_n\,\psi_n(r,R) \quad Eq.1.2$$

Where $\psi_n(r,R)$ is the wave function depending on the electrons coordinates r and nuclear coordinates R at the electronic state n, E_n is its eigenvalue and $\hat{H}$ is the molecular Hamiltonian independent on time.
In this case, the time-dependence of the eigenfunction of the Hamiltonian is given by $exp^{-iE_nt/\hbar}$: $\psi_n(r,R,t) = \psi_n(r,R)\ exp^{-iE_nt/\hbar}$ [1]

The Molecular Hamiltonian independent of time is [2]:

$$\hat{H}(r,R) = -\sum_{i=1}^{M}\frac{\hbar^2}{2m_e}\nabla_i^2 - \sum_{A=1}^{K}\frac{\hbar^2}{2M_A}\nabla_A^2 + \sum_{i=1}^{M}\sum_{j>i}^{M}\frac{e^2}{4\pi\epsilon_0|r_i - r_j|} + \sum_{A=1}^{K}\sum_{B>A}^{K}\frac{e^2 Z_A Z_B}{4\pi\epsilon_0|R_A - R_B|} - \sum_{i=1}^{M}\sum_{A=1}^{K}\frac{e^2 Z_A}{4\pi\epsilon_0|r_i - R_A|} \quad Eq.1.3$$

And can be written as [2]:

$$\hat{H}(r,R) = \hat{T}^e + \hat{T}^n + \hat{V}^{ee} + \hat{V}^{nn} + \hat{V}^{ne} \quad Eq.1.4$$

Where $\hat{T}^e$ and $\hat{T}^n$ refer to the kinetic energies for M electrons and K nuclei respectively, $\hat{V}^{ee}$, $\hat{V}^{nn}$ and $\hat{V}^{ne}$ are the potential energies representing the interactions between electrons or between nuclei and between nuclei and electrons respectively. Therefore, $\hat{V}^{ee}$ and $\hat{V}^{nn}$ are repulsive Coulomb interactions and $\hat{V}^{ne}$ is an attractive one.

1.2 Born-Oppenheimer approximation

The Born-Oppenheimer Approximation (BOA) is used to simplify the time-independent Schrödinger equation (Eq. 1.2). Since the nucleus of an atom, so the protons and neutrons, are almost 2 000 times heavier than the electrons, their motion is slower than the motion of the electrons. When the nuclei are moving, the electrons can be considered to instantaneously adapt to the new position of the nuclei. We can then separate the motions of the electrons and nuclei into two individual wave functions as follow [1]:

$$\psi_n(r,R) \approx \phi_n^{elec}(r;R)\,\chi_n^{nucl}(R) \quad Eq.1.5$$

Where n refers to the electronic state, $\phi_n^{elec}(r;R)$ is the electronic wave function where the position of the electrons r depends implicitly on the position of the nuclei R and $\chi_n^{nucl}(R)$ is the nuclear wave function.
The positions of the nuclei are not fixed, but since their motion is slow, the electrons will adapt instantaneously to the new geometry of the system. The Born Oppenheimer Approximation is an adiabatic approximation meaning that the electrons and nuclei are decoupled [1].
From this approximation, we can deduce two things. On one hand, the electrons are submitted to the statical potential of the nuclei (attraction). On the other hand, the nuclei are moving in the potential energy of the electrons defined by their motion.

1.3 Potential energy surface

A potential energy (PE) is defined by the energy of the electrons that implicitly depends on the positions of the nuclei and of the Coulomb repulsion between the nuclei. It represents the potential energy of the nuclei for the different nuclear geometries of the system under

investigation. For a molecule containing N atoms, the dimensions of the potential energy are 3N-6 [1]. For a diatomic molecule, the potential energy will be represented as a curve (PEC) and for a N>2 molecule, the potential energy will be a hypersurface and is called potential energy surface (PES). To define the potential energy surface, the electronic Hamiltonian and its eigenstates are required [1]:

$$\hat{H}^{elec} = -\sum_{i=1}^{N}\frac{\hbar^2}{2m_e}\nabla_i^2 + \sum_{i=1}^{N}\sum_{j>i}^{N}\frac{e^2}{4\pi\epsilon_0|r_i - r_j|} + \sum_{A=1}^{K}\sum_{B>A}^{K}\frac{e^2 Z_A Z_B}{4\pi\epsilon_0|R_A - R_B|} - \sum_{i=1}^{N}\sum_{A=1}^{K}\frac{e^2 Z_A}{4\pi\epsilon_0|r_i - R_A|} \quad Eq.1.6$$

The above equation is similar to the total Hamiltonian (eq 1.3) but does not include the kinetic energy of the nuclei. We can therefore rewrite the equation 1.6 as follow:

$$\hat{H}^{elec} = \hat{T}^e + \hat{V}^{ee} + \hat{V}^{nn} + \hat{V}^{ne} \quad Eq.1.7$$

Treating the nuclei as classical particles is, depending on the system under investigation, a good alternative to a full quantum mechanical treatment. The nuclei being heavier than the electrons, they are treated classically and are moving on the PES defined by the electronic energy. Knowing this potential energy, one can then solve classical equation of motion for the nuclei.

The basic classical equations of motion for the nuclei are the Newton equations [2]:

$$F_{\boldsymbol{A}} = M_A\ddot{R}_A \quad with\ A = 1, \dots N \qquad Eq.1.8$$

Where F_A, M_A and $\ddot{R}_A$ are the force, mass and acceleration applied on the nuclei A.

For an isolated system, the force applied on the nuclei A is the negative derivative of the potential energy V(**R**) depending on the position of the nuclei A and is expressed as [2]:

$$F_A = -\frac{dV(\boldsymbol{R})}{dR_A} \quad Eq.1.9$$

Knowing that a molecule is made of several nuclei, their motion is coupled because the potential energy V(**R**) depends on all the coordinates. The force acting on the nucleus A depends also on the positions of the other nuclei in the molecule. Finally, we will obtain 3N coupled equations due to N the number of nuclei in the molecule and 3 cartesian coordinates (x,y,z).

Therefore, the potential energy for the electronic state n is given by:

$$V_n(\boldsymbol{R}) = E_n(\boldsymbol{R}) = \left\langle \phi_n^{elec} \middle| \hat{H}^{elec} \middle| \phi_n^{elec} \right\rangle \quad Eq.\ 1.10$$

The potential energy surface on which the nuclei will move is defined by solving the electronic time-independent Schrödinger equation [1]:

$$\hat{H}^{elec}\,\phi_n^{elec}(r;R) = E_n(R)\phi_n^{elec}(r;R) \quad Eq.1.11$$

There is one potential energy surface per electronic state n.

As discussed above, the potential energy is the variation of energy $E_n(R)$ of the energy of the electronic state n as a function of the positions of the nuclei [1].

Writing Eq. 1.8 more explicitly, we obtain a system for 3N coupled equations since the potential energy depends on all the Cartesian coordinates of the nuclei:

$$\begin{cases} F_{A,x}(t) = -\nabla_{A,x} V_n(\boldsymbol{R}) \\ F_{A,y}(t) = -\nabla_{A,y} V_n(\boldsymbol{R}) \\ F_{A,z}(t) = -\nabla_{A,z} V_n(\boldsymbol{R}) \end{cases}, \qquad A = 1, \dots, N \; Eq. 1.12$$

The right terms represent the forces acting on the nucleus A along the x/y/z-axis of the frame and is determined by computing the negative of the gradient of the potential energy surface depending on the coordinates of all the nuclei. [1,16].

Potential energy surfaces can be computed with model potentials called force fields (coupled harmonic or anharmonic potentials) or computed by solving the electronic Schrödinger equation for the geometries sampled during the reaction. This is what is done in 'on the fly' methods, or 'ab initio molecular dynamics', AIMD. In these implementations of classical molecular dynamics, the potential energy and the force on the nuclei (the gradient of the potential) are not pre-computed. They are computed only for the geometries of the nuclei reached when integrating the classical equations of motion for the nuclei (Eq. 1.12). The motion of the nuclei occurs on a single potential energy surface (on a single electronic state). For this reason, this type of nuclear dynamics is also called Born Oppenheimer (BO) dynamics [2].

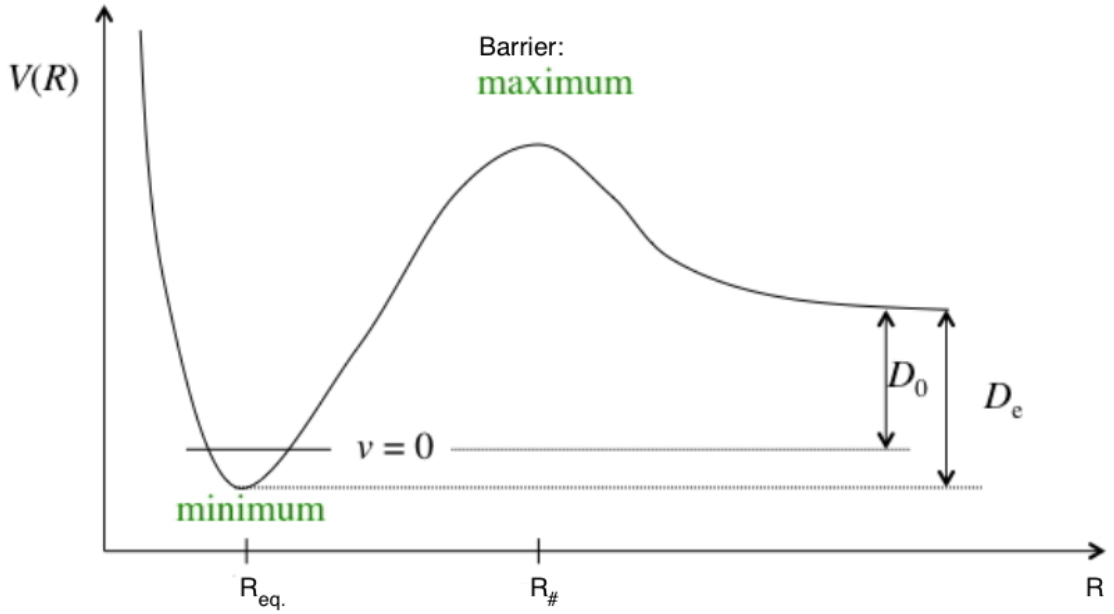

Fig. 1.1: Example of a PE curve for a diatomic molecule

Figure 1.1 shows the potential energy curve of a diatomic molecule. Two extrema are observable where the gradient depending on the nuclear coordinate R is equal to zero, so we have $\nabla[V(R)] \equiv \frac{dV}{dR} = 0$. Therefore, the force acting on the nuclei is expressed as $F = -\frac{dV(R)}{dR}$, so when the gradient is equal to zero, the force F is also equal to zero. These points are called stationary points.

A minimum is observed at R_{eq} where $\frac{dV}{dR} = 0$ meaning that no force is acting on the nuclei. The second derivative $\frac{d^2V}{dR^2}$ is positive, meaning the geometry corresponds to a stable point on the PEC. It is the equilibrium geometry of the molecule.
The second extremum corresponds to a maximum at $R_{\#}$. In this case, $\frac{dV}{dR} = 0$ and the second derivative $\frac{d^2V}{dR^2}$ is negative. This maximum is an unstable point and corresponds to the maximum of the barrier for dissociation along the internuclear distance.
The potential energy curve is therefore very important to give information about the equilibrium structure of a molecule, the asymptote for dissociation, the thermochemistry, but also the minimum energy that needs to be provided in order to dissociate it and the rate of the reaction.
Potential energy surface is based on Born-Oppenheimer approximation with the separation of the total wave function into nuclear and electronic wave functions (Eq. 1.5).
This approximation is valid if the potential energies from different electronic states are not close in energy. Otherwise, there is nonadiabatic interactions between the PES where the BOA breaks down [1].

1.4 Conical intersection

In photochemistry, excited electronic states are involved and treating the motion of nuclei and electrons separately is not possible due to an important coupling. This is a nonadiabatic coupling induced by the nuclear motion that leads to the breakdown of the BOA. In this case, two PES are close in energy or crossing each other. They are coupled and the motion of the electrons can no longer be separated from the one of the nuclei. Regions of non-adiabatic interactions involve a change of the electronic configuration of wave function while the nuclear motion is occurring [2,17].
A minimum energy conical intersection corresponds to the crossing point between the two electronic states. At this point, the two electronic states are degenerate and the energy difference between two states is therefore equal to zero [2,17]. In the region of geometries around the conical intersection, we can observe a radiationless transition between the two electronic states due to the nonadiabatic coupling.

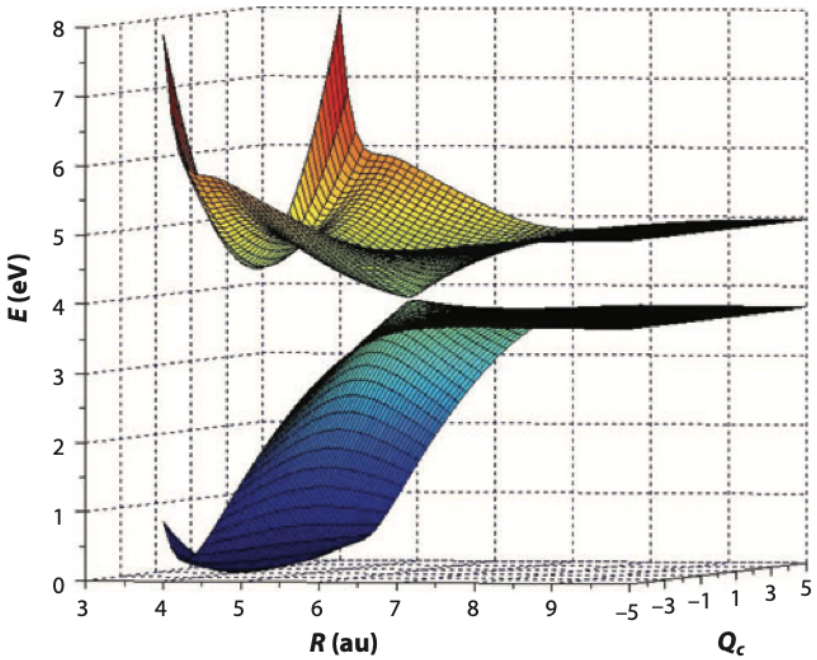

Fig. 1.2: Representation of a conical intersection [18]

1.5 Surface hopping

As discussed in 1.4, for molecules that are excited by UV light, several excited states of the molecule may be involved in the dynamic. In this case, considering one PES is not possible. Especially when two or more electronic states are close in energy, the BOA is not valid anymore because non-adiabatic transitions between these states are occurring [17] .

Surface hopping is a semi-classical dynamic method proposed by Tully and Preston in the 70s [2]. This methodology for nuclear dynamics is well-adapted for non-adiabatic excited-state dynamics. Here, the nuclei are moving in an adiabatic way along a single PES but non-adiabatic transitions are allowed from a PES to another when the two PES are coupled (close in energy). The trajectory *hops* from an adiabatic PES to another around for example a conical intersection [2]. The coupling between electronic states is defined as [17]:

$$f_{IJ}^{\alpha}(\boldsymbol{R}) = \left\langle \phi_I^{elec}(r;R) \middle| \nabla_{\alpha} \phi_I^{elec}(r;R) \right\rangle \quad Eq.\,1.13$$

Where ϕ_I^{elec} and ϕ_J^{elec} are the electronic wave functions at the electronic states I and J. $f_{IJ}^{\alpha}(\boldsymbol{R})$ is the coupling vector in 3N dimensions (the 3N cartesian coordinates of the nuclei). This coupling leads to an extra term in the nuclear Hamiltonian, the non-adiabatic coupling (NAC) term:

$$\widehat{H}^{NAC} = \sum_{I} \sum_{\alpha} \vec{f}_{IJ}^{\alpha}(\boldsymbol{R})\, \vec{P}_{\alpha}(\boldsymbol{R}) \frac{1}{M_{\alpha}} \quad Eq.\ 1.14$$

From this equation, we can see that the NAC term depends on the coupling vector defined in eq. 1.13 and the vector of the momentum of the nuclei. It also depends on the mass of the nuclei M_{α}.

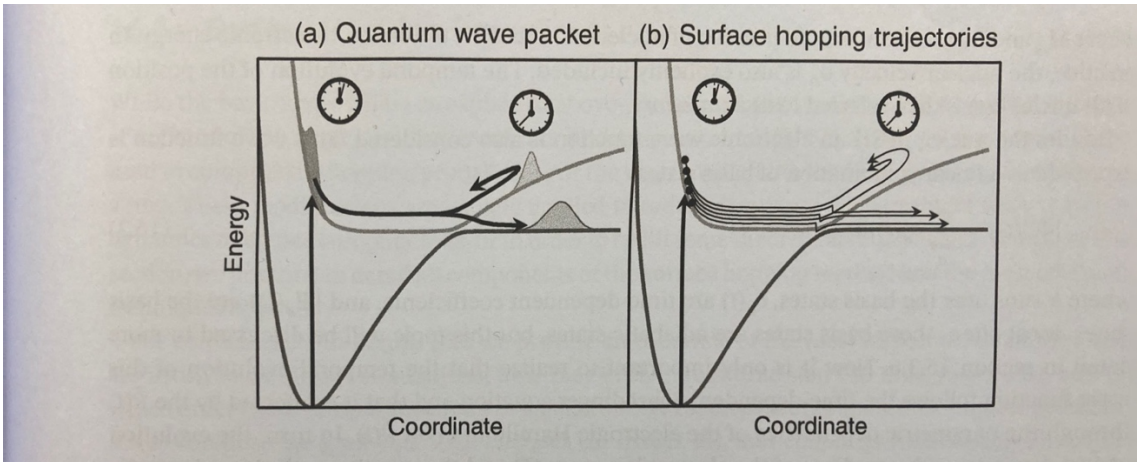

Fig. 1.3: Comparison of quantum packet (a) to surface hopping trajectories (b) [2]

Figure 1.3 illustrates the difference between a quantum wave packet which corresponds to a fully quantum description by solving the TDSE (Eq. 1.1) for coupled electronic states and the semi-classical surface hopping approximation. In surface hopping we assume that an ensemble of trajectories for which the nuclei are treated classically can describe a nuclear wave packet. This is achieved by designing a set of initial conditions for the equations of motion (1.12) by sampling the geometries of the ground state vibrational wave packet. By averaging over the positions of the nuclei given by the ensemble of trajectories at each time step, we can simulate the probability of the localization of a quantum wave function. In Fig. 1.3 a) the wave packet is split into two parts after crossing the non-adiabatic (avoided crossing) region. From a quantum point of view, after the avoided crossing, the wave function occupies simultaneously the two electronic states but has a slightly higher probability to occupy the lower state. To simulate this process semi-classically, in Fig 1.3 b), five trajectories have been promoted at the highest state initially, to simulate an ultrafast Franck Condon (FC) excitation to this excited electronic state. Then at the crossing point, three of them are hopping to the lowest state while the two others stay at the highest one. Classically, a system cannot occupy two states at the same time. So, if we average over the trajectories after the crossing point, we get a higher probability for the system to be in the lowest state, in agreement with the quantum result. Using this method, it is possible to simulate a quantum phenomenon using classical mechanics [2].

In surface hopping, nuclei are described classically with the Newton's equation of motion (Eq. 1.12).
Concerning the electrons, they are described with the time-dependent electronic wave function represented as a linear combination of electronic basis states [19]:

$$|\phi^{elec}(t)\rangle = \sum_{n} c_n(t)\ |\phi_n(t)\rangle \quad Eq.1.15$$

Where n corresponds to all the states forming the basis set, $|\phi_n(t)\rangle$ are the electronic wave function of all the states n obtained by solving the electronic time independent Schrödinger equation, eq. (1.2) for the geometry R of the nuclei. The coefficients $c_n(t)$ are the time dependent amplitudes on each electronic state n at time t. The electronic energy defined in equation 1.2 depends on the adiabatic electronic states. The potential energy in Eq. (1.12) above depends on the basis of electronic states set chosen. In fact, the basic set chosen for the electronic states will influence the shape of the PES. Another basis of electronic states are

the diabatic states which can be more advantageous because the coupling between electronic states is a potential term while it appears as a momentum term in the adiabatic basis set. The purpose is to select a basis set as large as possible to obtain results as accurate as possible without being too expensive on a computational point of view [19,20].

Surface hopping approximation method is very useful because it is possible to deal with large molecules without solving the molecular time-dependent Schrödinger equation (Eq. 1.1) by computing several trajectories as a function of time to simulate the time evolution of the molecular quantum wave packet. However, using a classical description means that we neglect quantum effects like tunneling or nuclear (and electronic) interferences. Therefore, surface hopping can be used when these quantum effects are negligeable in order to converge to the exact result that would be obtained by using quantum dynamics [2].

2. Objectives

The main goal of this study is to investigate the isotope effect on the competition of D_2 and D loss in the deuterated ethylene cation, $C_2D_4^+$. Therefore, this study is based on the previous one reported by M. Lucchini, B. Mignolet et al. about hydrogenated ethylene cation [8].
In this previous article, experimental results were explained by surface hopping simulations.

Investigating the photochemistry of polyatomic molecules, so their reactivity induced by a light excitation, is very complex and there are not yet black box dynamical methodologies. The reason is that the light excitation must be in the femtosecond range, we are then talking about ultrafast dynamics that can take place on several coupled electronic states [8].
Nevertheless, understanding the mechanisms of dissociation of a molecule or which step is determinate can be very useful.
The ethylene cation is the simplest π-radical system, and its dissociation is characterized by two main dissociating pathways leading to two different final products [10].
The two dissociations are given below with their corresponding threshold leading to H or H_2 loss which leads to the acetylene ($C_2H_2^+$) and vinyl ($C_2H_3^+$) cations respectively:

$$C_2H_4^+ \rightarrow C_2H_2^+ + H_2 \quad 2.62\ eV \quad Eq.2.1$$
$$C_2H_4^+ \rightarrow C_2H_3^+ + H \quad 2.70\ eV \quad Eq.2.2$$

As we can see, the two reactions have close energy thresholds meaning that one reaction will not be favored over the other one by energetic constraints. In other words, both reactions will compete [10].

In order to investigate the photochemistry of $C_2H_4^+$, both experiments and theoretical simulations were performed.

2.1 Experimental results for $C_2H_4^+$ dynamics

Experimentally, a 15-fs extreme ultraviolet pulse (EUV), with an energy band width laser pulse of 0.24 eV, was used together with an infrared pulse in a pump-probe set up for investigating on the dynamic relaxation of $C_2H_4^+$ [8].
First, the EUV pulse (the pump) was used to ionize the neutral ethylene molecule to the four lowest states of the ethylene cation: $\tilde{X}$ being the ground state and $\tilde{A}$, $\tilde{B}$ and $\tilde{C}$ being the excited

states. The EUV pulses is produced by High Harmonic Generation. The wavelengths of the 9th (H9), the 11th (H11) and the 13th (H13) pulses correspond to a photon energy of 14 eV, 17 eV and 20.2 eV respectively. They allow to access the four lowest electronic states of the cation as shown in Fig. 2.1 [8].

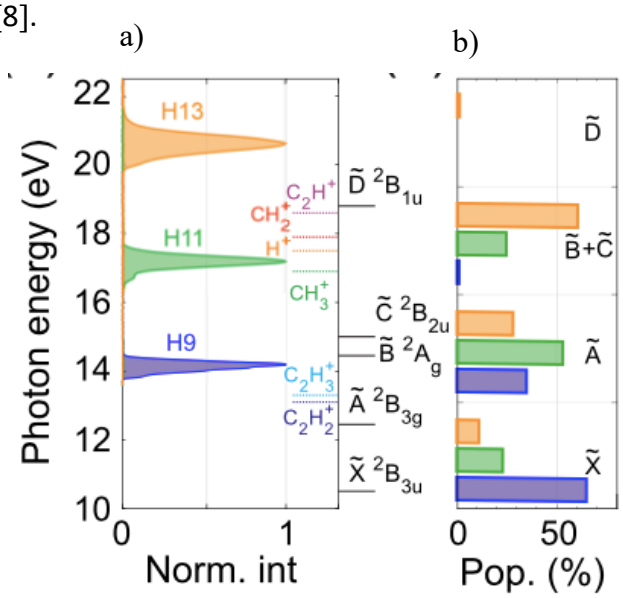

Fig 2.1: a) Photon energy of the three harmonics with the vertical transition energies (black horizontal lines) and the fragment appearance potentials (colored dotted lines) and b) expected initial state populations. Adapted from [8].

In fig. 2.1 a), the photon energy of the H9, H11 and H13 harmonics is compared to the energies of the ground state $\tilde{X}$ and the three lowest excited states $\tilde{A}$, $\tilde{B}$ and $\tilde{C}$ of the ethylene cation. The energies of the harmonics are such that it is possible by a vertical ionization to access more than one electronic state of the cation.
We can therefore anticipate the excitations that will occur (Fig. 2.1 b). For the H9 we will mostly obtain $C_2H_4^+$ at the ground state $\tilde{X}$, H11 will primarily generate the first excited state $\tilde{A}$ and H13 will primarily excite $C_2H_4^+$ at the two higher electronic states $\tilde{B}$ and $\tilde{C}$ [8].

The yields in fragments created after the relaxation were also analyzed (Fig 2.2)

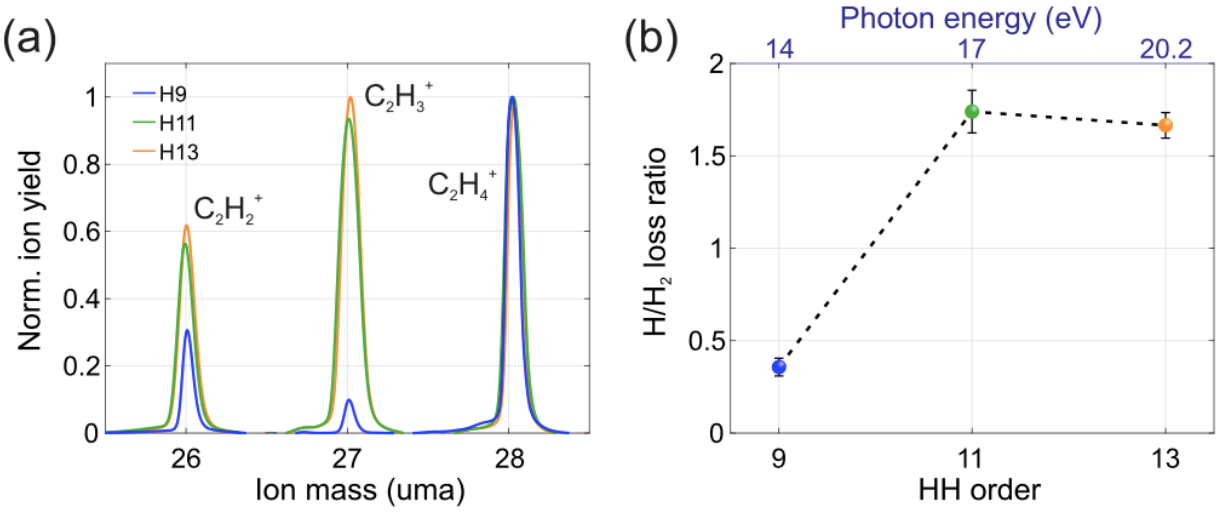

Fig 2.2: a) Normalized heavy fragment yields obtained with H9 (blue), H11 (green), and H13 (orange) EUV pulses and b) H/H_2 loss ratio after excitation with the three pulses. Adapted from [8].

Fig. 2.2 a) reports the normalized yields in the heavier fragments obtained with different ionization energies. Using H9 will mainly lead to parent $C_2H_4^+$ in agreement with fig. 2.1 a) and does not promote its fragmentation. Regarding H11 and H13 ionization, they will lead to a fragmentation of the parent $C_2H_4^+$ cation with H and H_2 loss. The ratio of H/H_2 loss is plotted in fig 2.2b as a function of the ionization energy. Ionizing with H9 leads essentially to the production of the parent $C_2H_4^+$. We observe a small ratio H/H_2 loss meaning that the H_2 loss is favored over the H loss for H9. On the contrary, ionizing with H11 and H13 leads to a larger amount of fragmentation and to a larger ratio of H/H_2. The H loss is favored for higher ionization energies [8].

To understand better the relaxation dynamics of $C_2H_4^+$ from an experimental point of view, a pump-probe scheme was used. The "pump" corresponds to the ionization of the molecule with the different harmonics while the "probe" uses an IR pulse to interrogate the fragmentation mechanisms that occur after the pump pulse. The IR pulse has an intensity of $I_{IR} = 3.3 \times 10^{12}$ W/cm^2 and a duration of 15 fs which corresponds to an energy band width of 0.24 eV. The ions produced are analyzed as a function of the delay between the "pump" so the initial excitation and the "probe" as follow [8]:

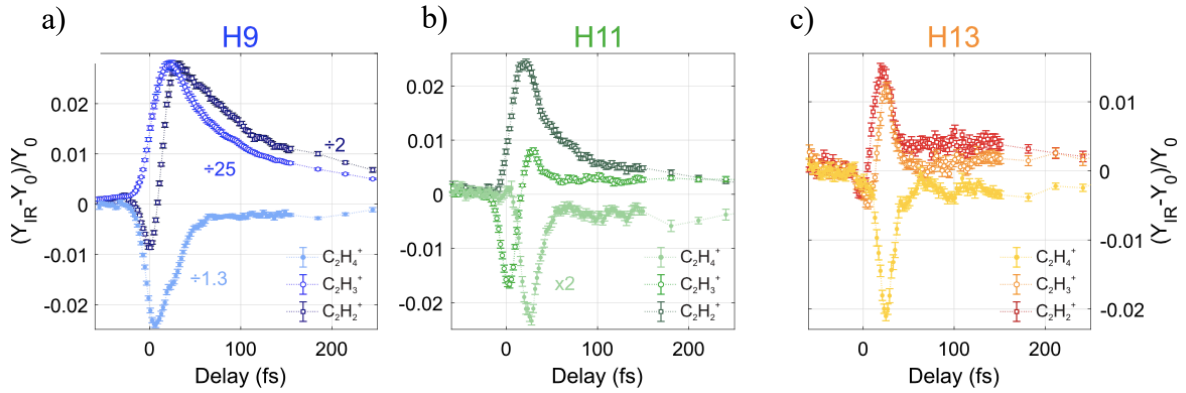

Fig 2.3: (from left to right) differential ion yields as a function of the delay between the EUV and IR pulse as obtained with H9, H11 and H13. Adapted from [8].

The differential fragment yield is defined as follow:

$$\Delta Y\,(\tau) = \frac{Y_{IR}(\tau) - Y_0(\tau)}{Y_0(\tau)} \quad Eq.2.3$$

Where τ is the pumb-probe delay, Y_{IR} and Y_0 are the ion yield measured when the IR field is turned on and turned off respectively [8].

The differential ion yield is plotted in figure 2.3 as a function of the delay between the "pump" and the "probe". We can observe a decrease of the parent $C_2H_4^+$ and an increase of the children $C_2H_2^+$ and $C_2H_3^+$. Looking at figure 2.3 a), we observe a bleaching of the parent meaning that the IR pulse provides enough energy to the parent for it to dissociate. Concerning 2.3 b) and c), we observe a bleaching of the parent as for 2.3 a) but with a delay of around 20 fs. The IR pulse is providing energy to the system and so favors the fragmentation. Comparing a with b and c, the effect of the IR pulse is less visible after 100 fs delay for H11 and H13. Concerning 2.3 a) the effect of the IR pulse is visible until 220 fs [8].

These experimental results were also explained using theorical approach and more precisely surface hopping and Born-Oppenheimer molecular dynamics. The simulation starts after the cation is excited by the different harmonics.

2.2 Theoretical results for $C_2H_4^+$ dynamics

From a theoretical point of view, the relaxation from the four excited states of ethylene cation is modelled by starting an ensemble of classical trajectories on each of the four states D0, D1, D2 and D3. By plotting the relaxation of the trajectories started on the different electronic states as a function of time, one obtains fig. 2.4 [8]:

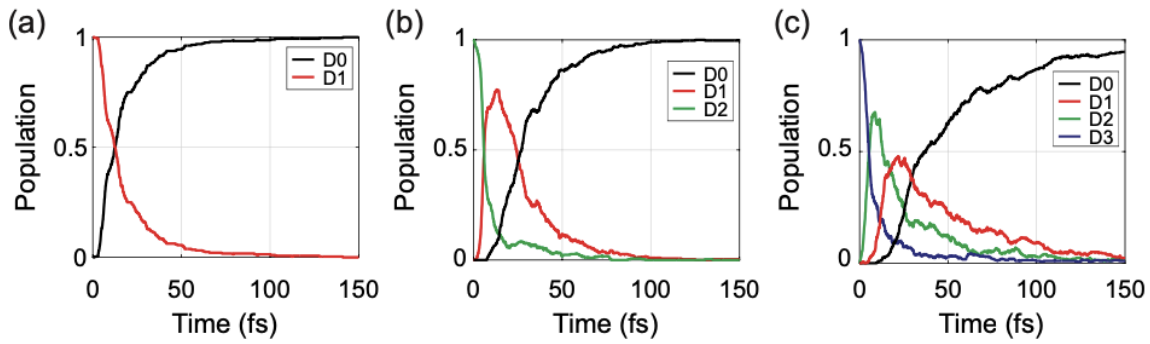

Fig. 2.4: (from left to right) Nonradiative relaxation from D1 (a), D2 (b) and D3 (c) excited state [21].

From the above figure, we can observe that the excited state time life (so the time for half of the trajectories to reach the ground state D0) is 12.6 fs, 27.1 fs and 36.6 fs for the trajectories starting from D1, D2 and D3. So, the higher the excited state, the longer the relaxation to the ground state will be [21].

The dissociation of $C_2H_4^+$ will occur on the ground state. Once the trajectories are relaxed to the ground state for at least 10 fs, the simulation is switched to BOMD (see section 3.1.2) in order to monitor which fragmentation occurs on D0 depending on the excited state of the initial conditions [8].

Table 2.1: Simulated Dissociation Yield after 2 ps of dynamics starting from the states D0 to D3 [8].

	dissociation yield		
initial state	$C_2H_4^+$	$C_2H_3^+$	$C_2H_2^+$
D0	100%	0%	0%
D1	96%	4%	1%
D2	43%	41%	16%
D3	31%	55%	13%

Table 2.1 reports the yield of fragments obtained after starting the simulation at D0, D1, D2 and D3. Starting from D0 and D1 will lead to essentially the parent cation $C_2H_4^+$, meaning that dissociation is not or only slightly occurring. Concerning the fragments obtained after starting from D2 and D3, the percentage of $C_2H_4^+$ will decrease with the increase of the excitation energy. In this case, when the system will relax through conical intersections, no energy is released. So once at the ground state, the system has enough energy to dissociate [8].

The following table compares the dissociation yields obtained in experiments and in the simulations.

Table 2.2: ion yield observed and computed depending on the initial excitation [22]

	State accessed			Ion yield observed				Ion yield computed			
	D0	D1	D2+D3	$C_2H_2^+ + H_2$	$C_2H_3^+ + H$	$C_2H_4^+$	Ratio $C_2H_3^+/C_2H_4^+$	$C_2H_2^+ + H_2$	$C_2H_3^+ + H$	C_2H4^+	Ratio $C_2H_3^+/C_2H_4^+$
H9	40%	40%	20%	23%	8%	77%	10%	3%	11%	86%	13%
H11	5%	5%	90%	23%	38%	38%	100%	13%	44%	43%	100%
H13	5%	5%	90%	23%	38%	38%	100%	13%	44%	43%	100%

In Table 2.2, we see that the ion yield obtained in experiments and simulations are similar with a difference of approximately 15%. Concerning the ratio of the yields $C_2H_3^+/C_2H_4^+$, the experimental and computed results are also similar, which means that the initial conditions chosen for the simulation are adequate to describe the experimental results [22].

After the ionization of the ethylene cation, an IR pulse is used to probe the relaxation and fragmentation dynamics. The IR pulse will re-excite the molecule and therefore enhance the fragmentation yield due to the energy that it provides to the system. In ref. [8], it was shown that the IR pulse re-excites the ethylene cation that has relaxed to D0 to the D3 state when it is 3-photon resonant with D0. This conclusion was supported by analyzing the dependence of the transition dipole moment between D0 and D3 on the elongation of the CC bond and the opening angle HCH for the trajectories, Fig. 2.5.

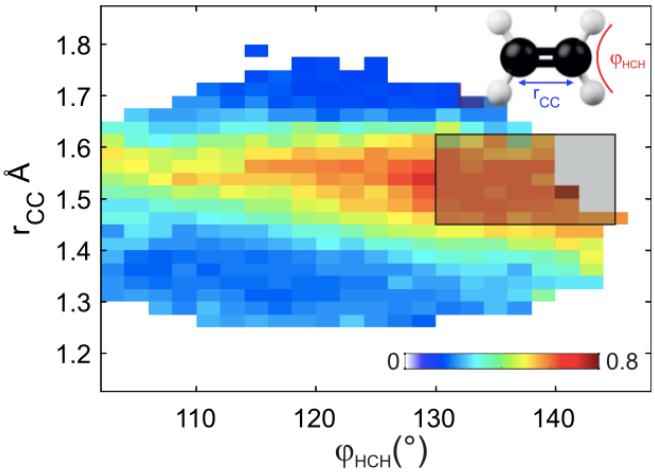

Fig. 2.5: Probability to have a transition dipole moment between D0 and D3 depending on the elongation CC and opening angle HCH. Adapted from [8].

The dipole strength is the largest when the CC bond is elongated between 1.45 Å and 1.60 Å and the angle HCH is opened between 130° and 145°. The larger the dipole strength, the higher is the probability to have a transition from D0 to D3 with the IR pulse. Therefore, the delay for the parent bleaching observed in Fig 2.3 for H11 and H13 ionization corresponds to the time at which the molecule is in the optimized geometry on D0 so that it can be re-excited to D3 [8].

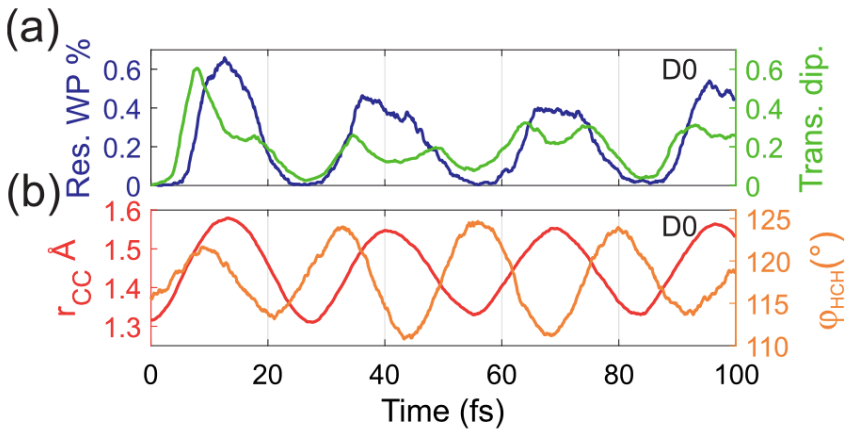

Fig 2.6: a) fraction of trajectories that are 3-IR-photon resonant from D0 to D3 (blue curve) and the mean transition dipole moment from D0 to D3 (green curve), b) corresponding value of CC bond (red curve) and HCH opening angle (orange curve). Adapted from [8].

The fraction of trajectories that are 3-IR-photon resonant as well as the transition dipole from D0 to D3 is reported in fig. 2.6 a). The corresponding values of the CC bond elongation and the opening angle HCH is also reported in fig 2.6 b) depending on time. The elongation of the CC bond and the opening angle of HCH are both large in the first 10 fs after the excitation by EUV. M. Lucchini, B. Mignolet et al. [8] reported that the transition dipole from D0 to D3 will be the highest for an elongation of the CC bond and an opening of the HCH angle (see fig 2.5). Therefore, in the first 10 fs, the transition dipole is large and so more than 60% of the trajectories can be re-excited to D3.

Computing the relaxation dynamics of the ethylene could also give information about the geometry of the molecule when it hops from a potential energy surface to another. When the simulation starts from D1 and D2, the cation goes through the planar conical intersection most of the times while it relaxes through planar and twisted conical intersections (CI) when the dynamics starts at D3. M. Lucchini, B. Mignolet et al. [8] also observed that the molecule will be easily excited by the IR pulse when it comes from the twisted conical intersection due to a favorable geometry with a CC bond already elongated and an HCH angle open. Therefore, coming back to D0 through the twisted CI will favor the re-excitation to D3 and will enhance the fragmentation yield after re-exciting with an IR pulse [8].

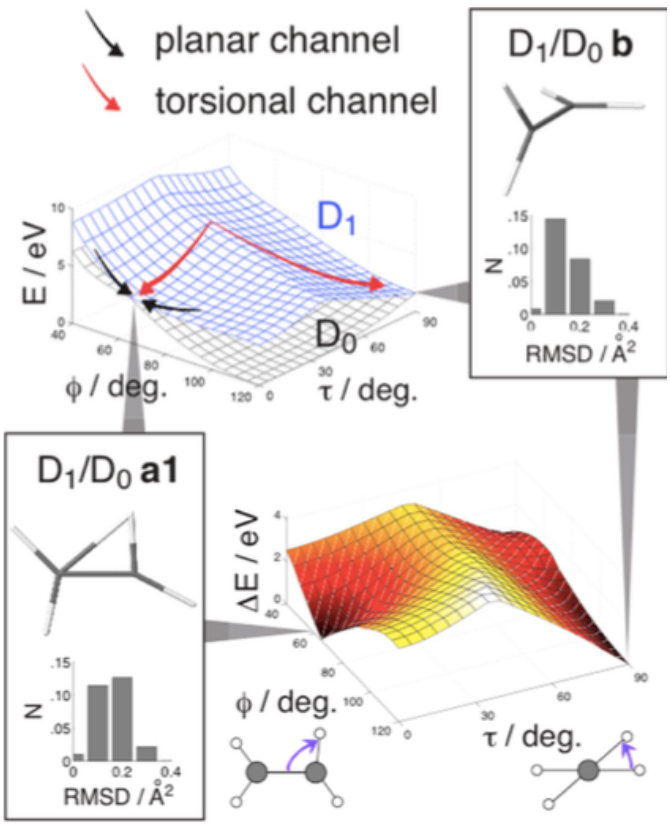

Fig 2.7: Schematic view of the pathways leading to the planar and the twisted CI [10].

Fig. 2.7 shows the two pathways leading for the relaxation of the ethylene cation. The first one is the twisted CI with a dihedral angle equal to 90° and the other one is the planar CI where the dihedral angle is equal to 0 [10]. It was also observed that a relaxation through the planar configuration will lead to mostly H_2 loss and the twisted relaxation path is leading to essentially H loss [10,8].
To conclude, the initial ionization energy as well as the relaxation pathway will determine which fragmentation will occur.

2.3 Isotope effect

Isotopes are species that have the same atomic number but a different mass number due to a different number of neutrons within these species. For example, hydrogen (H) and deuterium (D) are isotopes. They have the same atomic number (Z=1) but a different number of neutrons which is 0 for the hydrogen and 1 for the deuterium. Therefore, the mass number of hydrogen is 1 and the one of deuterium is 2.
Replacing an atom in a molecule by one of its isotopes will influence the reaction rate of each step of the reaction but not the potential energy surfaces, electronic dipoles and non-adiabatic coupling since the electronic Hamiltonian (Eq. 1.6 above) does not depend on the mass of the nuclei. Examining the changes in the yields in fragments induced by isotopic substitution is a way to understand in more details the different reactions steps that occur and which step of the reaction is kinetically determinant [23,24].

In this study, the four hydrogen atoms in the ethylene cation were replaced by deuterium.

2.4 Experimental results for $C_2D_4^+$ dynamics

In order to investigate the isotope effect on the relaxation dynamics of $C_2D_4^+$, the same experiment was performed than the one with $C_2H_4^+$ but with a slightly higher intensity of the IR probe pulse equal to 3.5 x 10^{12} W/cm^2 (which is 6% higher) in order to obtain clearer signals. It was checked that the IR intensity pulse does not have an impact on the dynamics [14].

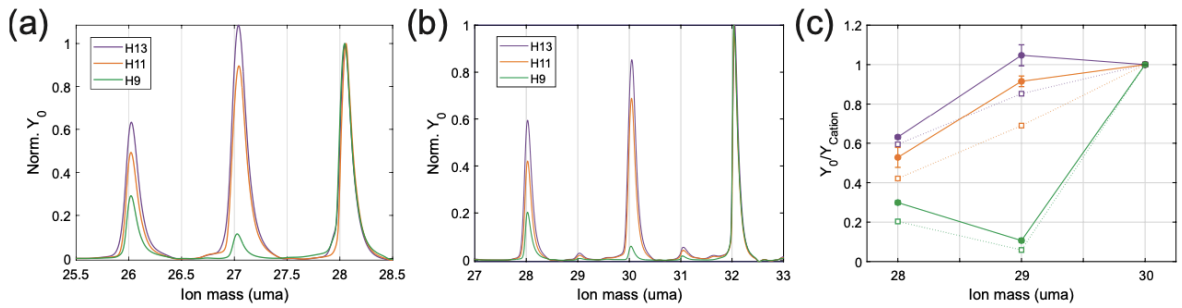

Fig. 2.8: Heavy fragment yields obtained with H9 (green), H11 (orange), and H13 (purple) for ethylene cation hydrogenated (a) and deuterated (b) and C) H/H_2 loss ratio after ionization with the three different harmonics (*full lines are the ethylene hydrogenated results and the dashed line are the deuterated one*) [14].

The relative yields of heavy fragments divided by their cation signals for $C_2H_4^+$ and $C_2D_4^+$ are plotted in Figures 2.8 a and b. This figure reports the fragmentation yield for the EUV ionizing pulse (the pump) only, so before applying an IR pulse. Looking at fig. 2.8 c), there is a higher probability for a fragmentation to occur with the hydrogenated ethylene cation than the deuterated one.

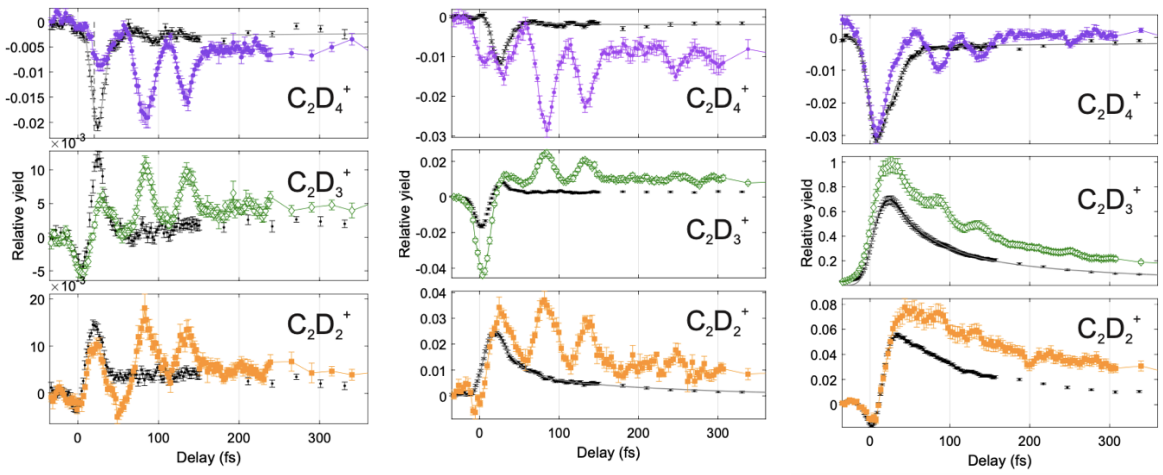

Fig 2.9: first column: relative ion yield as a function of pump-probe delay after H13 ionization, second column: relative ion yield as a function of pump-probe delay after H11 ionization, third column: relative ion yield as a function of pump-probe delay after H9 ionization. *The black line represents the results obtained with ethylene cation hydrogenated*. Adapted from [14].

In Figure 2.9, for an ionization with H13 and H11 (left and middle columns), the oscillations as a function of the pump-probe delay are more pronounced for the deuterated ethylene cation than for the hydrogenated one. The parent cation bleaching signal is also shifted to a longer

time for $C_2D_4^+$. These oscillations of the parent bleaching and the fragment yields are in-phase. With the H9 ionization, the oscillations of the deuterated fragments follow qualitatively the ones of their equivalent hydrogenated fragments but with higher amplitudes and for longer delay times. A shift to longer time delays is not observed for the first peak [14].

2.5 Theoretical results for $C_2D_4^+$ dynamics

The relaxation dynamics of the deuterated ethylene cation was computed. The main purpose is to first compare the simulation results with the ones obtained experimentally and second compare them to the results obtained for $C_2H_4^+$ in order to investigate the isotope effect.
The IR pulse is not explicitly included in our simulations.

3. Computational method

As the first purpose of this study is to investigate the isotope effect on the dissociation of the ethylene cation, we used the same computational method as the previous study for the hydrogenated ethylene cation, $C_2H_4^+$ reported by M. Lucchini, B. Mignolet et al. [8].
The nonradiative relaxation of the ethylene cation have been simulated using the Surface Hopping including Arbitrary Couplings (SHARC) software [25] and Born-Oppenheimer Molecular Dynamics (BOMD) [26].

3.1 Molecular dynamics

3.1.1 SHARC

The SHARC is an ab initio molecular dynamics program developed by the González Group at the University of Vienna [25]. This software is a general approach of trajectory Surface Hopping method suitable for any type of couplings (non-adiabatic coupling, spin-orbit coupling, dipole-moment laser field coupling, …). In SHARC, the total electronic Hamiltonian is diagonalized including these couplings and is expressed as follow [19]:

$$\widehat{H}^{SHARC-elec} = \widehat{H}^{elec} + \widehat{H}^{additional} \quad Eq.3.1$$

Where $\widehat{H}^{elec}$ is the electronic Hamiltonian also called Molecular Coulomb Hamiltonian and has the form of the equation 1.6 and $\widehat{H}^{additional}$ is the additional Hamiltonian due to the coupling terms between electronic states. In this study, we consider the NAC term (Eq. 1.14).

a- Electronic structure

We first calculated the optimized geometry of the deuterated ethylene C_2D_4 and the frequencies of the normal modes at the ground state in order to set up the initial conditions. For this step, the quantum chemistry software MOLPRO which has an interface with SHARC was used. We used the SA-CASSCF method implemented in MOLPRO. State Average Complete Active Space Self-Consistent Field (SA-CASSCF) is a multi-determinant theory that determines the electronic structure of several electronic states simultaneously and which is suitable for computing nonadiabatic couplings between the electronic states included in the computation [19]. For the geometry optimization, we considered the neutral molecule of deuterated ethylene, C_2D_4, and computed at the SA (7)-CASSCF (9MO, 12electrons) with 6-311G (d,p) basis set. Concerning the dynamics simulation of the cation, we computed $C_2D_4^+$ with the same

basis set as the neutral but with one electron less which gives: SA (7)-CASSCF (9MO, 11electrons) with 6-311G (d,p) basis set [8].

b- Initial conditions

We assume that the ionization by the EUV pump pulse is a sudden ionization process. In this approximation, the vibrational ground state of the ground electronic state of the neutral is projected on the potential energy surfaces of the electronic state of the cation, D0, D1, D2 and D3. The Wigner distribution of the ground electronic state of the neutral was used to describe the vibrational wave packet and generate initial conditions of nuclear positions (R) and their velocity (p). From the Wigner distribution, geometries and momenta are selected randomly (see Fig. 3.1) in the phase space and form a set of initial conditions that are independent [2].

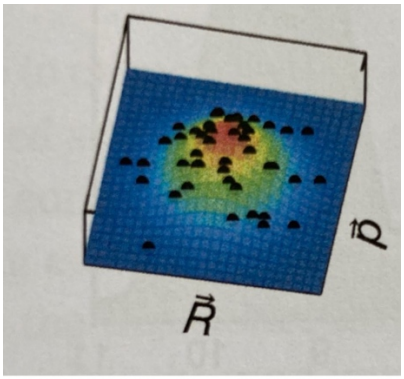

Scanned with CamScanner

Fig. 3.1: Initial condition generated using Wigner distribution function. Adapted from [2].

In this study, 300 sets of initial conditions were generated using the Wigner sampling method. Then, the initial excited states, so the electronic state where the molecular dynamical simulation will start, were selected. The neutral ethylene molecule was ionized to the four lowest states of the cation, so D0/D1/D2/D3 with 300 sets of initial conditions in each state [8].

c- Dynamics simulations

After setting up the initial conditions, the dynamics simulation was performed with SHARC. Afterwards, every trajectory was analyzed independently. If the trajectory has relaxed to the ground state for at least 10 fs, we switched to Born-Oppenheimer Molecular Dynamics (BOMD).

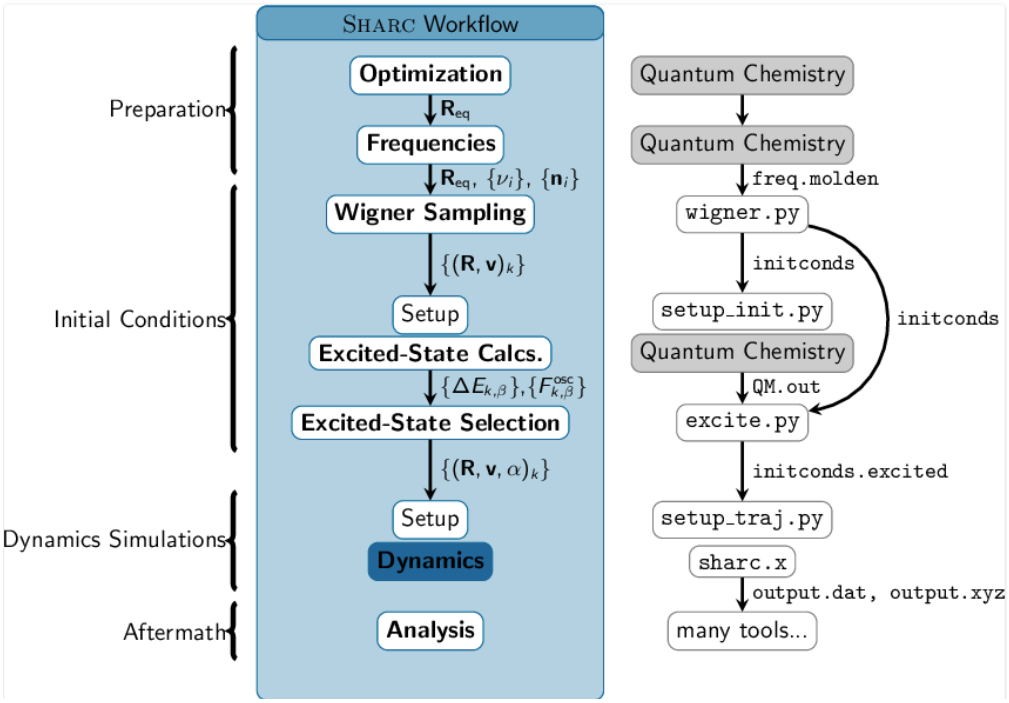

Fig. 3.2: Typical workflow for a trajectory Surface Hopping simulation in SHARC software [28] *on the left side is shown the procedure followed and on the right side the corresponding script in SHARC that are used.*

3.1.2 Born-Oppenheimer Molecular Dynamics method (BOMD)

In BOMD, the nuclei are restricted to move on the ground state potential energy surface. Therefore, no transition to another electronic state is allowed [16]. The equations 1.11 and 1.12 are used with the electronic state n equal to 0 as the system is moving on the ground state only.

In the case of this study, we used BOMD implemented in Gaussian 16 [26] with the DFT B3LYP level structure and 6-311G++(d,p) AO basis set. The larger basis of AO is necessary to describe the long-range interactions along the dissociative pathways.
By using this approximation, we assume that the probability of a nonradiative transition to a higher electronic state is very low after a relaxation of 10 fs on the ground state, and therefore we neglect this process. The dissociation of the ethylene cation will then occur on the ground state [8].
The initial conditions for the BOMD simulations were set to the values of the positions and the momenta of the last step of the SHARC simulation on D0.
We encountered a large number of crashes of trajectories in the SHARC simulation in the first dozen of fs of the dynamics. We come back on this point below.
The trajectories that crashed before relaxing to D0 were restarted in SHARC using the last geometry and velocity of the trajectory until the relaxation to D0.

3.2 Processing data

First, the frequencies of the normal modes at the ground state of $C_2H_4^+$ and $C_2D_4^+$ were compared to each other in order to find how the normal modes are affected by the isotope

substitution. For this, we analyzed the frequencies obtained during the "preparation" step in SHARC.
According to Hooke's law for a harmonic oscillator, the vibrational frequency of a diatomic depends on the reduced mass [23]:

$$\nu = \frac{1}{2\pi}\sqrt{\frac{K}{\mu}} \quad Eq.3.2$$

With

$$\mu = \frac{m_A \times m_B}{m_A + m_B} \quad Eq.3.3$$

where ν is the frequency, K the force constant, μ is the reduces mass. In the case of a polyatomic molecule, we have 3N-6 normal modes which each correspond to a harmonic oscillator but with a reduced mass different from the simple expression for a bond stretching as given in Eq. 3.3. By replacing the hydrogen (H) by the deuterium (D) in the ethylene cation, we can compare the values of the normal mode frequencies and deduce the isotope effect on each mode. In the case of a polyatomic molecule, the force constants K, which are the elements of the Hessian matrix, given by the second derivative of the electronic energy, will be the same between $C_2H_4^+$ and $C_2D_4^+$. As the potential energy V is determined by the electronic Hamiltonian which depends only on the charge of the nuclei and electrons and on the electronic mass, (protons and electrons), adding a neutron will in principle not change the force constants [23].
Applying equations 3.2 and 3.3 to a CH bond we have $\mu_D/\mu_H \approx 2$ so $\nu_D/\nu_H \approx \sqrt{2} \approx 1.4$. If the expression of the reduced mass is different from 3.3, the ratio can vary, this is why each normal mode is not affected in the same way by the isotope substitution.

Then, using Matlab and Python scripts, the trajectories from SHARC and BOMD were analyzed. We extracted the geometries, velocities, and energies of the trajectories. We analyzed from these trajectories:

- The configuration of the ethylene cation (planar or twisted) at the last jump to D0 electronic state. The cation was considered as twisted for a dihedral angle between 45° and 135°.
- The relaxation curves of the excited states starting from D1, D2 and D3
- The fragmentation that occurs in BOMD that can be either D_2 loss, D loss or no dissociation.
- The transition dipole moment between D0 and D3 and its correlation the coordinates of the nuclei

  The transition dipole moment is the electric dipole moment between an initial state *i* and a final state *f* is expressed as follow [1]:

  $$R_{i\to f} = \langle \psi_i | \hat{q} | \psi_f \rangle \quad Eq.3.4$$

  where $\hat{q}$ is the dipole moment and can be expressed as the sum of nuclear dipole moment and electronic dipole moment as follow:

  $$\hat{q} = \hat{q}^{elec}(r;R) + \hat{q}^{nucl}(R) \quad Eq.3.5$$

  And r and R refer to the electronic ad nuclear coordinates respectively.
  Therefore, by using the Born-Oppenheimer approximation (Eq. 1.5) we can rewrite the equation 3.4 [1]:

$$R_{i\to f} = \langle \psi_i | \hat{q} | \psi_f \rangle$$
$$= \left\langle \chi_i^{nucl}(R)\phi_i^{elec}(r;R) \middle| \hat{q}^{elec}(r) \middle| \chi_f^{nucl}(R)\phi_f^{elec}(r;R) \right\rangle$$
$$+ \left\langle \chi_i^{nucl}(R)\phi_i^{elec}(r;R) \middle| \hat{q}^{nucl}(R) \middle| \chi_f^{nucl}(R)\phi_f^{elec}(r;R) \right\rangle \quad Eq.3.6$$

Here, we are investigating in a transition between D0 and D3 which is a transition between two electronic states. Therefore, the contribution of the transition dipole moment coming from the nuclei is equal to 0 [1].

All of these data are compared to the ones obtained with $C_2H_4^+$ to deduce if there is an influence of the isotope substitution.

4. Results and discussion

4.1 Normal mode frequencies

First, the frequencies of the ground state of $C_2D_4^+$ and $C_2H_4^+$ in MOLPRO using the SA (4)-CAS-SCF (9,11) multideterminantal level with the 6-311G(d,p) AO basis set and in Gaussian with the DFT B3LYP functional and the 6-311++G(d,p) basis set in order to compare with the results of the MOLPRO calculation. The basis set used in the Gaussian computations is larger to compensate the fact that in DFT we use a single reference electronic wave function while the wave function is a multi-determinantal one in the MOLPRO computations.
The equilibrium geometry of the cationic ground state is twisted with a torsional angle equal to 28°.

Table 4.1: Frequencies of the normal modes of $C_2H_4^+$ and $C_2D_4^+$ ground state using a CAS-SCF level in MOLPRO and a DFT/B3LYP level Gaussian and isotope effect calculation.

Normal modes	Frequencies of $C_2D_4^+$ with B3LYP 6-311++G(d,p) basis set	Frequencies of $C_2D_4^+$ with CAS-SCF 6-311G(d,p) basis set	Frequencies of $C_2H_4^+$ with CAS-SCF 6-311G(d,p) basis set	Frequencies of $C_2H_4^+$ with B3LYP 6-311++G(d,p) basis set	Isotope effect
HCH out of plane twisting	431	373	524	552	1.40
HCH in plane rocking	570	632	879	808	1.39
HCH out of plan wagging	671	732	970	910	1.32
HCH out of plane wagging	884	941	1147	1081	1.22
HCH in plane scissoring	966	1047	1358	1218	1.24
CCH in plane rocking	974	1064	1320	1280	1.30
HCH in plane scissoring	1057	1158	1562	1452	1.35
CC stretching	1341	1484	1692	1531	1.14
CH symmetric stretching	2228	2365	3275	3132	1.38
CH symmetric stretching	2249	2428	3303	3134	1.36
CH asymmetric stretching	2373	2548	3401	3230	1.33
CH asymmetric stretching	2382	2551	3422	3247	1.34

The frequencies of the normal modes of the cationic ground state of $C_2H_4^+$ and $C_2D_4^+$ are reported in Table 4.1.

It can be seen in Table 4.1 that we obtain similar frequencies for $C_2H_4^+$ with a difference up to 11% with the different computation levels and for $C_2D_4^+$ the results differ up to 10% and about

15% for the first frequency corresponding to “HCH out of plane twisting”. However, in the literature, the frequency of the vibration HCH out of plane twisting is reported to be equal to 84 cm^{-1} for the $C_2H_4^+$ [29]. We obtained a frequency equal to 552 cm^{-1}. S-C.Chen, M-C Liu et al. [29] computed the frequencies of hydrogenated ethylene cation at the B3LYP level and obtained a frequency for the twisting normal mode equal to 558 cm^{-1}. This mode is strongly anharmonic and therefore not accurately described by the harmonic approximation used to compute the frequencies. The minimum of the potential energy surface for the torsional mode is very shallow.

The frequencies of $C_2D_4^+$ and $C_2H_4^+$ calculated at the CAS-SCF level were compared to investigate a possible isotope effect. An isotope effect occurs when the frequencies in the deuterated and in the hydrogenated species differ. As discussed above, on the basis of the ratio of the reduced masses of a C-H and C-D bonds, one expects a factor ≈ 1.4 in the vibrational frequency. From the table above, there is an isotope effect on essentially all the normal modes except on the CC stretching.

4.2 Surface hopping dynamics

The surface hopping dynamics of deuterated ethylene cation computed with SHARC was analyzed. The relaxation curves of the excited states starting from D1, D2 and D3 are plotted in Figure 4.1.

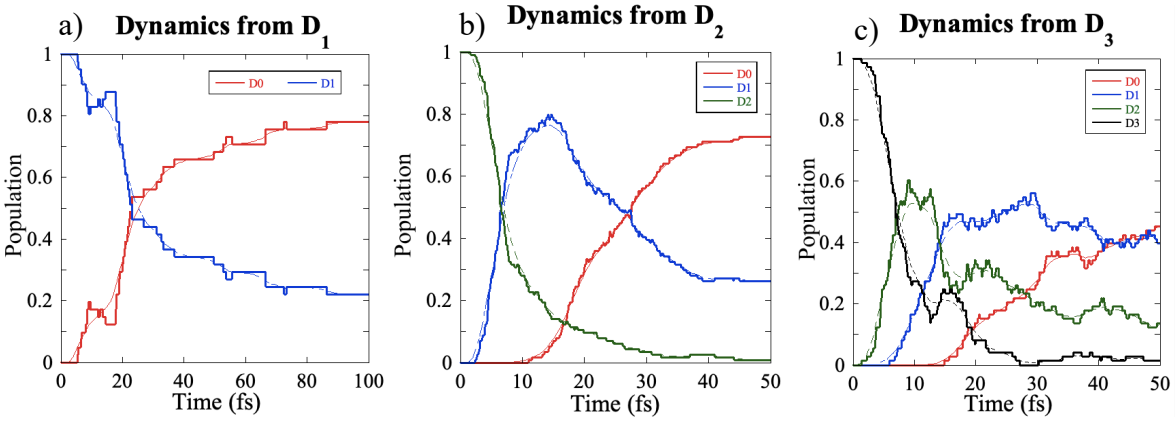

Fig 4.1: Non radiative relaxation curves from D1 (a), D2 (b) and D3 (c)

From fig 4.1 a), the excited state lifetime, so the time for at least 50% of the trajectories to relax to D0 is equal to 25,6 fs. When the simulation starts at D2, the excited states lifetime is equal to 27,6 fs. Concerning the dynamics starting from D3, 45,6% of the trajectories relaxed in D0 at 50 fs.

However, looking at fig 4.1 a), b) and c), we see that not all the trajectories of the ensemble have reached D0 at the end of the simulation time. In fact, a lot of trajectories crashed in the first 10 fs of the simulations. Two reasons can explain this. The first one is the set of initial conditions. The set of initial conditions was generated during the “preparation” step in SHARC, drawing a Wigner distribution from the vibrational wave function of the neutral C_2D_4 ground state and not the cation because we aim at simulating a vertical ionization process to each electronic state in the sudden photoionization approximation. Therefore, the guess for the electronic structure computation of the cation at a particular initial geometry was calculated from the electronic structure of the neutral which may explain the crash in the electronic structure computations. We are currently investigating this point. It appears that using more

recent version of MOLPRO (MOLPRO 2022), the electronic structure computation does not crash. But SHARC is only linked to the 2012 version of MOLPRO.
Comparing the dynamics starting from D1 for $C_2H_4^+$ and $C_2D_4^+$, the excited state lifetime is equal to 12,6 fs and 25,6 fs for $C_2H_4^+$ and $C_2D_4^+$ respectively. Concerning the dynamics starting from D2, the excited state lifetime is equal to 27,1 fs and 27,6 fs for $C_2H_4^+$ and $C_2D_4^+$ respectively. We therefore do not see an isotope effect in the relaxation time of D2. About D3 dynamics, no trajectories ran enough time to reach at least 50% of relaxation in D0. But 45,6% of the trajectories relaxed in D0 at 50 fs, if we compare this value to the one obtained with $C_2H_4^+$, so 36.6 fs, the time to relax is already longer than for the hydrogenated ethylene cation. If the trajectories ran longer which was not possible to check in the time available for this master thesis, we would obtain a larger relaxation time than for $C_2H_4^+$ [8,14].
The relaxation time is slower for the ethylene cation deuterated when the simulation starts at D1 and D3 meaning that there is an isotope effect on the dynamics. Concerning D2, the relaxation time is the same for $C_2H_4^+$ and $C_2D_4^+$ meaning that there is no isotope effect.

4.3 BOMD dynamics

When the trajectories in SHARC have relaxed at the ground state for more than 10 fs, the simulation were switched to BOMD in order to investigate the dissociation that will occur. The relative fragmentation yields for the different initial states are reported in the table 4.2.
As discussed above, a large number of trajectories crashed at the beginning of the SHARC simulation. For this reason, we could only restart a limited number of trajectories in BOMD. We had 47, 41 and 35 trajectories from D1, D2 and D3 respectively.

4.3.1 Fragmentation yields

Table 4.2: Simulated dissociative yield of dynamics starting from D0 to D3 in BOMD.

	Dissociation yields		
Initial state	$C_2D_4^+$	$C_2D_3^+$	$C_2D_2^+$
D0	100 %	0 %	0 %
D1	98 %	2 %	0 %
D2	65 %	30 %	5 %
D3	50 %	38 %	12 %

The fragmentation yields reported in table 4.2 vary considerably as a function of the initial state. The higher the energy of the initial, the lower the yield in parent $C_2D_4^+$. The same behavior is observed for the $C_2H_4^+$ case [8]. In fact, when the trajectories will relax to a lower electronic state through conical intersections, no energy is released. Consequently, when the system goes back to the ground state via a conical intersection, it has enough energy to dissociate.

Using the yields reported in Table 4.2 and the yields of ionization to the D0, D1, D2 and D3 by the three harmonics reported in fig 2.1 a), we get the fragmentation yields for the ionization by the three EUV pulses. They are reported in table 4.3. We also know from ref [8], that the ionization energy to remove an electron to the neutral ethylene is equal to 10.5 eV. Therefore, the different harmonics used to excite the ethylene are more energetic than the Ionization

Potential (IP) of the ground state. This excess of energy will allow the cation to be excited to higher excited electronic states than D0.

Table 4.3: Computed Fragmentation yields for the energy of the three EUV pulses.

	Fragmentation yields		
EUV pulse	$C_2D_4^+$	$C_2D_3^+$	$C_2D_2^+$
H9 (13,77 eV)	99 %	1 %	0 %
H11 (16,83 eV)	83 %	15 %	2 %
H13 (19,89 eV)	63 %	31 %	6 %

The highest the excitation energy, the more the parent ion will dissociate (as seen in table 4.2). The relative yield of D_2 loss is smaller than that of D loss. However, the percentage of D_2 loss is multiplied by 3 going from H11 to H13 ionization while the percentage of D loss is multiplied by 2. Note that there is an increase of fragmentation for H13 compared to H11 while for $C_2H_4^+$, the percentage of H and H_2 loss is the same for H11 and H13 excitation (see table 2.2).

A comparison of the fragment yield normalized by the relative cation yield between computed and experimental results for the deuterated ethylene cation is reported in table 4.4.

Table 4.4: Experimental and computed results of the fragment yield normalized by their relative cationic yield (the experimental results are extracted from fig 2.5 [14]).

	H9	H11	H13
Experimental D loss	0.08	0.7	0.85
Experimental D_2 loss	0.2	0.42	0.6
Computed D loss	0.01	0.18	0.49
Computed D_2 loss	0	0.02	0.1

For the deuterated ethylene cation, the experimentalists found out that both fragmentations, independently of the excited energy, are less likely to happen for $C_2D_4^+$ than for $C_2H_4^+$ (fig 2.8 c). In Table 4.4, the experimental yield for D loss is increasing with the increase of the excitation energy. Our computational results have the same behavior, but the D loss yield is smaller. So, the higher the excited energy, the more the deuterated ethylene cation will dissociate and loose D. Concerning D_2 loss, starting from H9, there is no dissociation, and the relative fragments yield is increasing from H11 to H13. Once again, this observation is in agreement with the experimental results. However, the computed fragmentation yields are smaller than the experimental ones. The fact that the computed fragmentation yields are systematically smaller is likely due to the fact that only ≈ 30 to 50 trajectories were run in BOMD.

4.3.2 Probing by the IR pulse

We analyzed the dependence of the transition dipole moment as a function of several coordinates to determine which is the optimized geometry of $C_2D_4^+$ to be re-excite from D0 to D3 by the IR pulse. In the following plots all the geometries of the trajectories are considered.

The geometry of the ethylene cation at the ground state with the numbering of the nuclei is reported in fig 4.2.

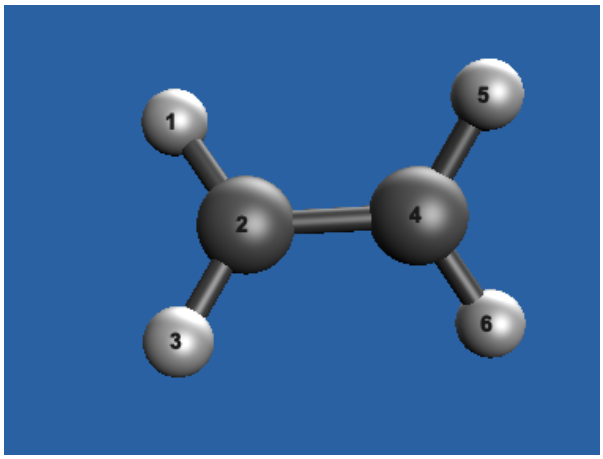

Fig 4.2: Optimized geometry of the deuterated ethylene cation at the ground state.

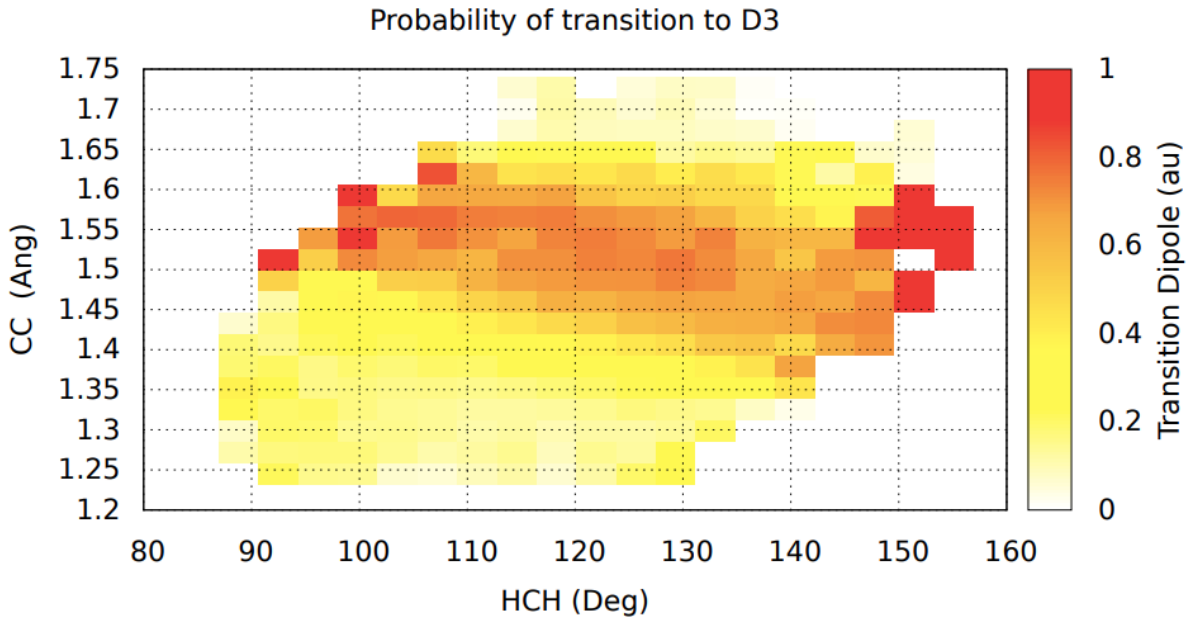

Fig 4.3: Heatmap of the computed D0/D3 transition dipole moment as a function of the CC bond and HCH angle.

In figure 4.3, the transition dipole moment is the highest for an elongation of the CC bond between 1.45 Å and 1.60 Å with an opening angle of the HCH bond between 110° and 150°. The same is observed for the $C_2H_4^+$ case (Figure 2.5).

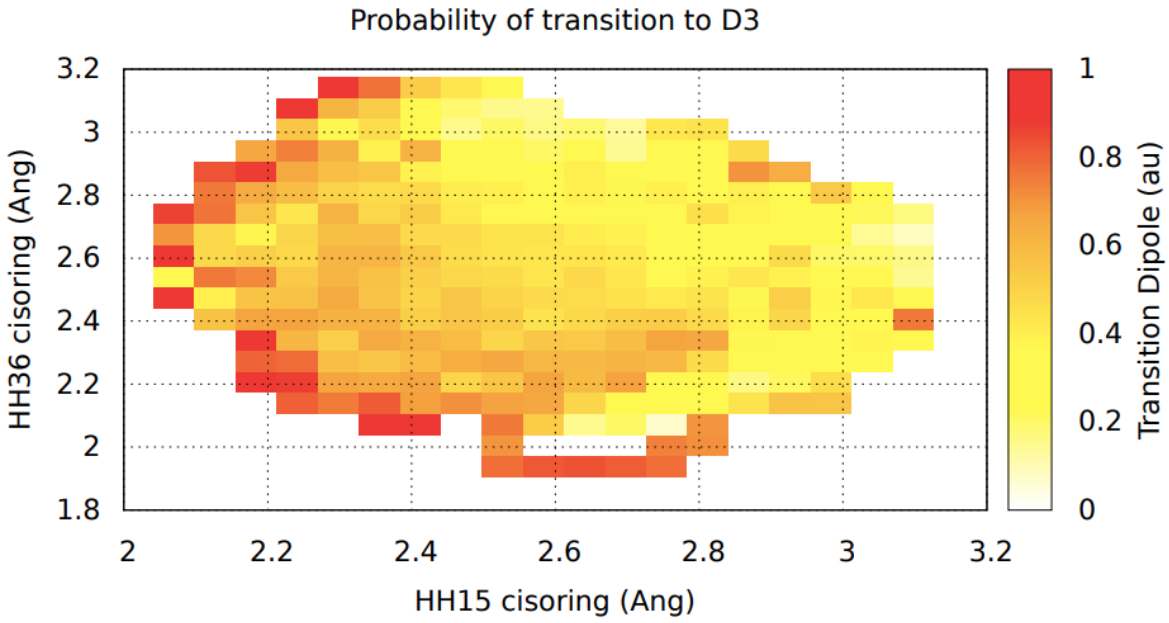

Fig 4.4: Heatmap of the computed D0/D3 transition dipole moment as a function of the distance between the hydrogen bonded with opposite carbons.

In figure 4.4, we see that there is the D0/D3 transition dipole is larger when both H-H distances are either large (3 Å) or small (2.3 Å). This motion corresponds to the HCH in plane rocking normal mode reported above (Table 4.1).

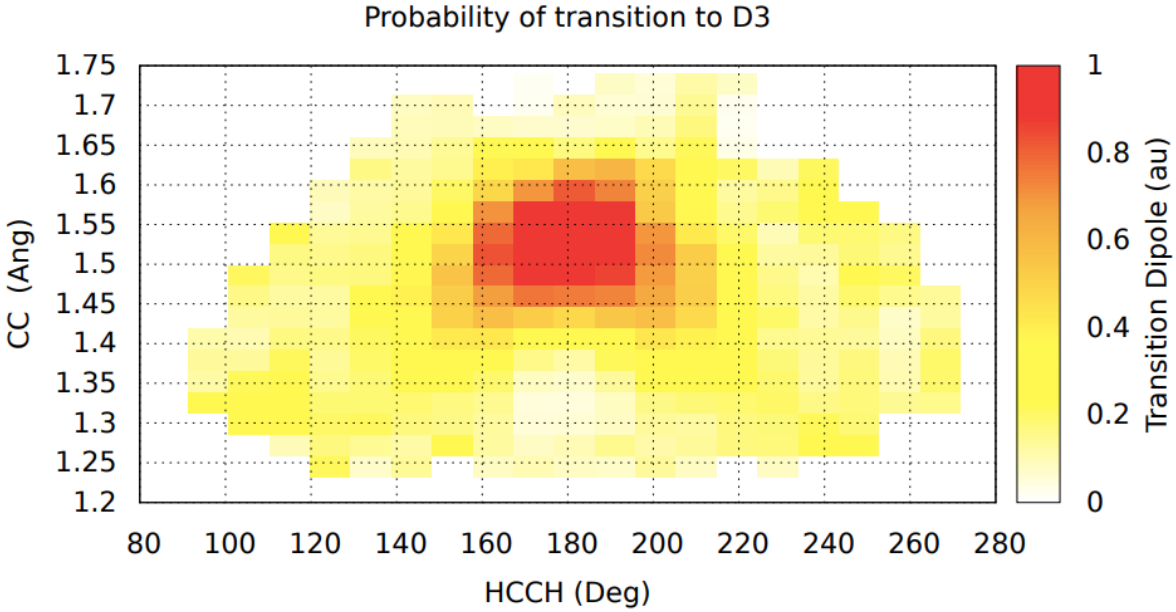

Fig 4.5: Heatmap of the computed D0/D3 transition dipole moment plotted as a function of the dihedral angle and the opening angle HCH.

Fig. 4.5 gives us one more information compared to fig. 4.3 ad 4.4. The transition dipole is the highest for a dihedral angle equal to 180°. However, we know from the previous study on $C_2H_4^+$ that the transition from D0 to D3 occurs when the molecule is twisted [8] because for a D3 initial state, most of the relaxation D1/D0 occurs through the twisted CI. This means that

the twisting motion on D0 is activated and could be a hindered rotation, which means that the geometry on D0 would pass periodically by the planar configuration. This is supported by the fact that the torsional barrier is very low, of the order of 350 cm^{-1}. [10,30] We note also that even if this is not the case, the value of the transition dipole for a twisted dihedral angle between 20-40 degrees is non-zero meaning that this transition is possible.

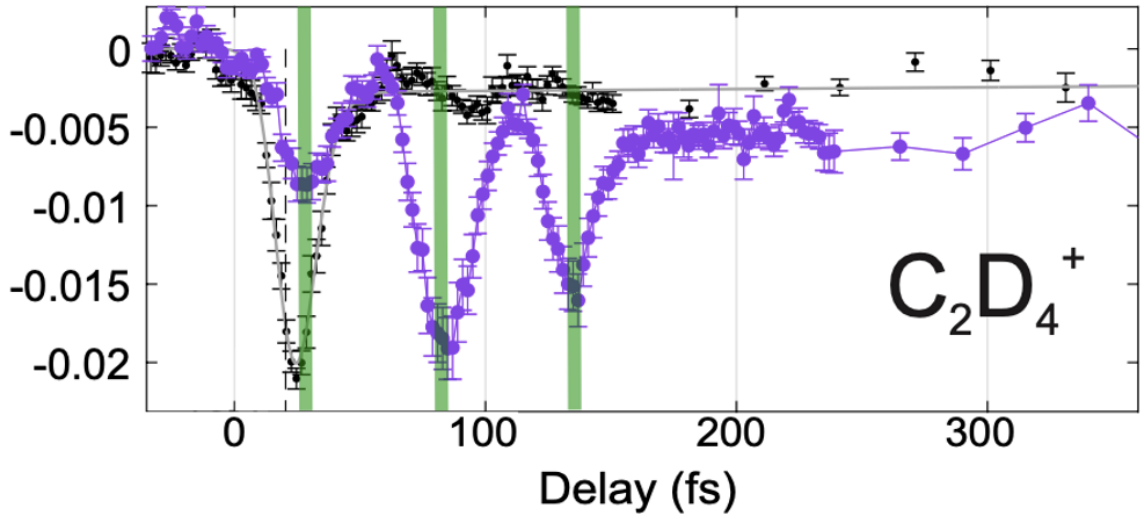

Fig 4.6: relative ion yield as a function of pump-probe delay after H13 ionization for the parent. *The black line represents the results obtained with ethylene cation hydrogenated*. Adapted from [14].

The relative experimental ion yield is reported in fig 4.6 as a function of the pump probe delay. For the deuterated ethylene cation, three pics are observed and corresponds to the bleaching of the parent. Three main regions are identified (green lines) at 15, 87 and 120 fs respectively. The time evolution of the fraction trajectories that are 3-photon D0/D3 resonant is plotted in fig 4.7.

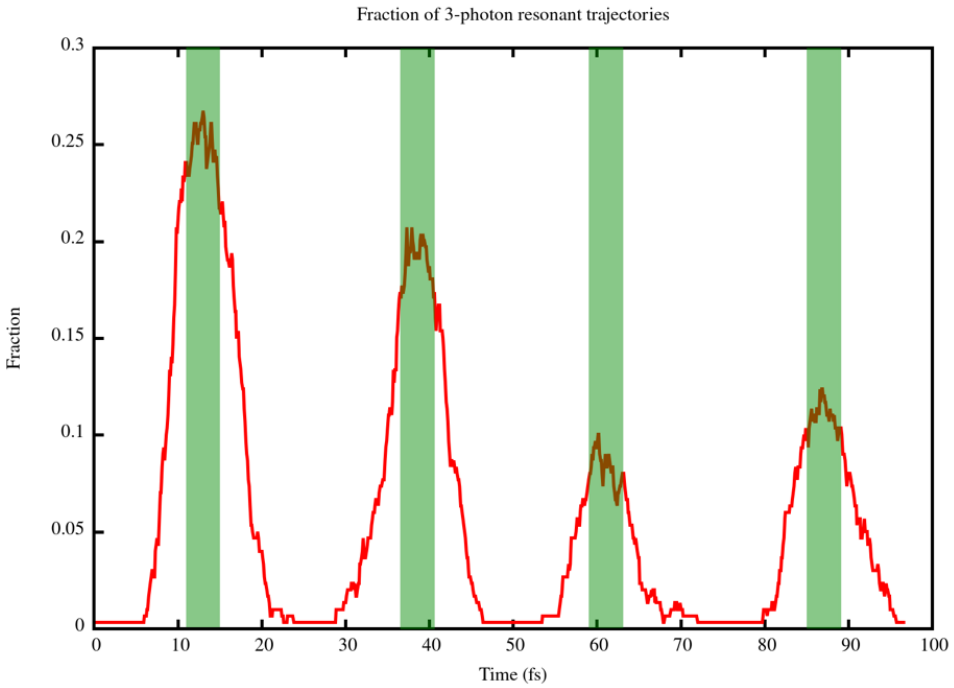

Fig 4.7: Time evolution of the fraction of the trajectories that are 3-IR photon resonant between D0 at D3.

The trajectories are 3-photon resonant at specific times during the simulation. The green lines are showing these regions. We can identify the trajectories 3-photon resonant around 13 fs, 27 fs, 62 fs and 87 fs for a percentage of 25 %, 20 %, 10% and 13% respectively. The time evolution of the mean transition dipole between D0 and D3 is reported in fig 4.8.

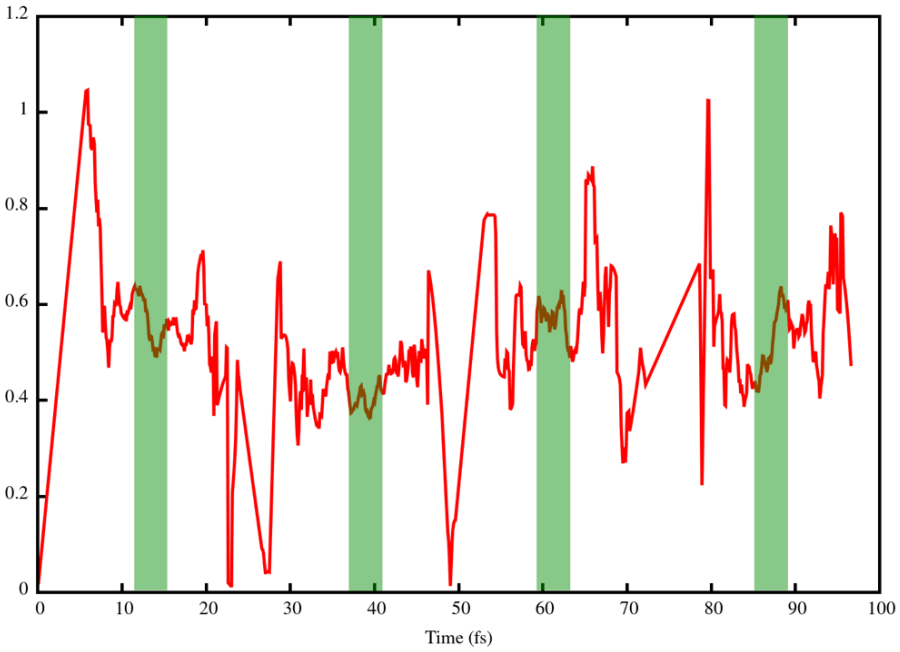

Fig 4.8: Time evolution of the mean transition dipole moment between D0 and D3 depending on time.

The transition dipole in the regions where the fraction of trajectories that are 3-photon resonant is high, is equal to 0.6, 0.45, 0.6 and 0.55 a.u. respectively. Taking ≈ 0.6 a.u. as a threshold for inducing a transition, we see that a re-excitation by the IR pulse could occur around 13 fs, 62 fs and 87 fs. We also know that re-exciting the cation at D3 will enhance the fragmentation [8]. Regarding fig 4.6, the two first bleaching of the parent matches with the times where we observe a higher probability of re-exciting the cation from D0 to D3. Therefore, the time evolution of the fraction of trajectories that is 3-photon resonant with D3 together with the constraint of having a large value of the transition dipole when the fraction is maximum could explain the oscillations of the yields observed experimentally as a function of the delay time. We also observe one peak where the transition dipole is equal to 0.6 around 62 fs but no bleaching of the parent is reported in fig 4.6. The time evolution of the coordinates for which we presented heatmaps of the transition dipole is plotted in fig 4.9.

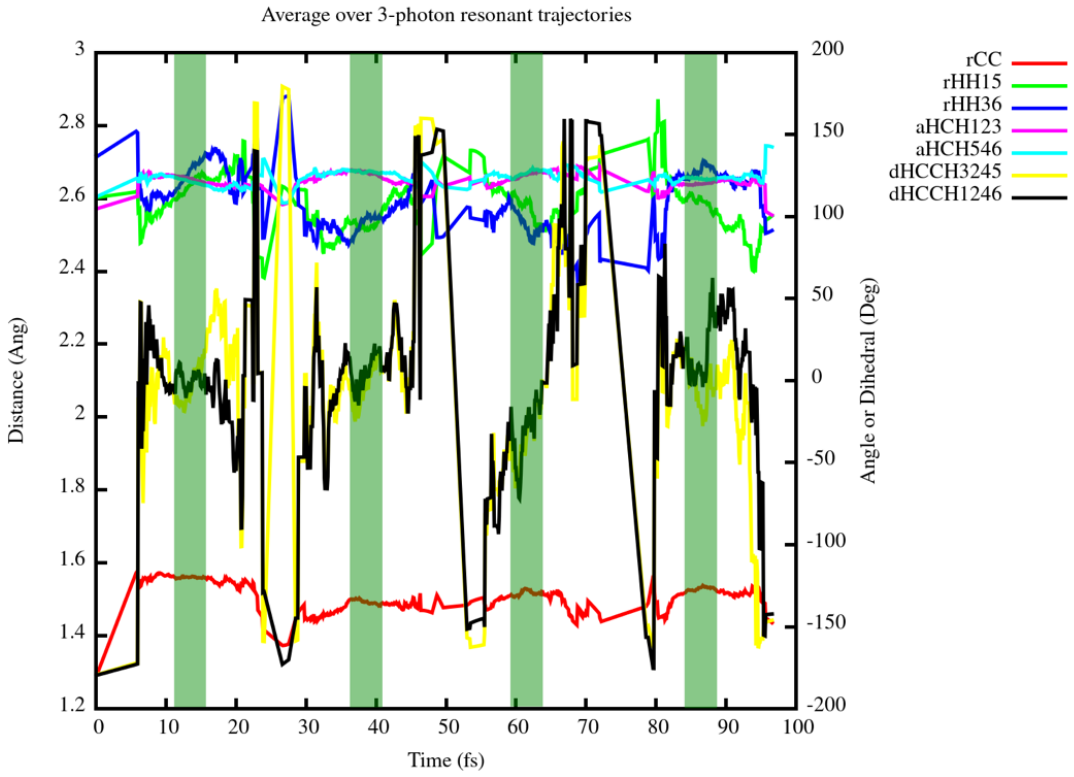

Fig 4.9: Mean values of CC bond (red curve), HH15 distance (green curve), HH36 (dark blue curve), angle HCH (purple curve), dihedral angle HCCH3245 (yellow curve), dihedral HCCH1246 (black curve) depending on time.

When the trajectories are 3-photon resonant, the angle of HCH is around 120° and the dihedral angle is around 180° except for the peak around 62 fs where it is slightly twisted. The CC bond is around 1.55 Å and is therefore in the range mentioned above to observe a large enough transition dipole (fig 4.3). Concerning the distance between the hydrogens bonded to opposite carbons, it can be either large (2.7 Å) or shorter (2.5 Å). Considering all these coordinates, their values are in the range observed before to have a maximum in the value of transition dipole (see fig 4.3, 4.4, 4.5).

In order to analyze the peak observed at 120 fs, the simulation time should be extended to 200 fs. It will then be possible to investigate more in these oscillations. The simulation time

should be also extended to 200 fs for the computed results of the hydrogenated ethylene cation. More trajectories should be run in order to get a better statistics and smoother curves as a function of time.

4.3.3 Relaxation paths

After analyzing each trajectory independently, we are able to deduce which conical intersection is responsible for the last jump from D2 to D1 and from D1 to D0 for the trajectories starting from D1, D2 and D3 excited states.
From D1, most of the trajectories relax through the planar conical intersection as observed for the hydrogenated ethylene cation. [8]
Concerning the dynamics from D2, the last hop from D2 to D1 is 54% through the planar CI and 46% through the twisted CI and the last hop from D1 to D0 is 66% through the planar CI and 34% through the twisted CI. According to M. Lucchini, B. Mignolet et al. [8], when the simulation starts on D2, the planar configuration intersection is favored for $C_2H_4^+$ dynamics. In the case of $C_2D_4^+$, the planar configuration is only slightly favored. However, as observed above, the relaxation time of D2 is not affected by the isotope substitution. The motions at the planar CI involve less the D atoms than those at the twisted CI. This might explain why there is no isotope effect on the relaxation time of D2 since the fraction of trajectories that relaxes through the planar conical intersection is higher than for D3. This conjecture needs to be verified by running more trajectories to get better statistics.
About the dynamics from D3, the last hop from D2 to D1 and from D1 to D0 is 86% twisted and 83 % twisted respectively. For the relaxation from D3, the twisted configuration is favored. This observation is the same as the one reported by M. Lucchini, B. Mignolet et al. as they found that the twisted configuration is predominant for the relaxation starting at D3.

4.3.4 Mechanisms for H loss and H2 loss

We begin by summarizing what is known about the mechanisms for H loss and H_2 loss for the ethylene cation.
According to J.C. Lorquet, C. Sannen and G. Raseev [11], two rearrangement processes can happen, evolving along two different dissociation pathways [12] on D0 which are schematically shown in figure 4.10.

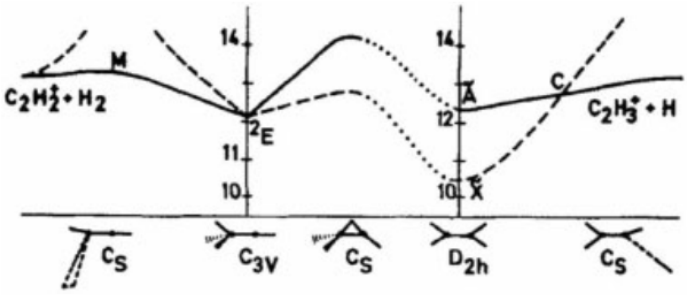

Fig 4.10: Reaction pathways of ethylene cation that leads to two different fragmentation products on the potential energy surface of the ground state and the first excited state [11].

On the left-hand side of Fig. 4.10, the ethylene cation is isomerized to form the ethylidene $HCCH_3^+$ stable cation after passing by a bridge transition state. This transition will lead to H_2

loss. On the right-hand side, the ethylene cation will lose a hydrogen by elongating the CH bond leading to its rupture [12].

For the dynamic starting from D2, 73% of the trajectories which lost D passed by the ethylene intermediate, 18% by the ethylidene and 9% through the bridge transition state. About the trajectories leading to D_2 loss, all of them (100%) passed by the ethylidene intermediate.

For the dynamic starting from D3, the observations are more heterogenous. Concerning the trajectories which lost D, 50% dissociate after passing by the ethylene intermediate, 30% through the ethylidene and 15% through the bridge configuration. For D_2 loss, 75% of the trajectories dissociate through ethylidene 25% through another mechanism not mentioned in [12] corresponding to two deuterium from opposite carbon nuclei that are recombined to form D_2.

Most of the trajectories from D2 are dissociating following what is presented in fig 4.10. Concerning the trajectories started from D3, just half of the ones which loose D are following the classical path and the rest is following different ones.
As we are using deuterium, the nuclei are moving slower on the potential energy surface on the ground state. Therefore, some conical intersections can possibly not be reached and another dissociating paths can be opened. This is probably the reason why not all of the trajectories are following the classical dissociating path to lead to either D or D_2 loss. These conclusions also need to be confirmed by running a larger number of trajectories.

Conclusion and perspectives

We investigated the isotope effect on the competition between D and D_2 loss of deuterated ethylene cation ionized to its four lowest electronic states using semi-classical dynamics.
The isotope substitution affects all the vibrational normal modes that involve the motion of H atoms on D0. The C-C stretching mode is only slightly affected.
We computed semiclassical surface hopping dynamics for $C_2D_4^+$ using the SHARC software, starting ensemble of classical trajectories on each four electronic states. The relaxation time of the excited states D1 and D3 is found to be longer for $C_2D_4^+$ than for $C_2H_4^+$, while the relaxation time of D2 is not affected. D_2 and D loss occur for the dynamics started on D2 and D3 for about 50% of the trajectories. No dissociating trajectory was obtained on D0 and only a few dissociate on D1. Also, the higher the energy of the initial state, the more the D_2 loss is favored. Overall, the isotope substitution decreases the fragmentation yields and both experimental (figure 2.8c) and computational results are in agreement on this point.
In the experiments, the dynamics is followed in a pump-probe set-up. The variation of the fragmentation yields is found to present high amplitude oscillations as a function of the delay time in the first 150 fs (figure 2.8). These oscillations in the fragment yields are much more pronounced for $C_2D_4^+$ than for $C_2H_4^+$ for which a single peak can be securely experimentally characterized. In order to understand the origin of these oscillations for $C_2D_4^+$, we followed the approach used in ref [8] for explaining the first peak in $C_2H_4^+$. We propose that the effect of the IR probe pulse is to re-excite the population that has relaxed to the ground state via a 3-photon process. This re-excitation is favored when two conditions are fulfilled (i) the energy difference between D0 and D3 corresponds to three IR photon. (ii) the geometry of this fraction of trajectories that are 3-photon resonant with D3 is such that we have a high value

of the transition dipole between these two states. Therefore, a bleaching peak of the parent cation $C_2D_4^+$ will occur when we have a maximum in the fraction of trajectories on D0 that is 3-photon resonant and when the transition dipole to D3 is maximum. We find in the case of $C_2D_4^+$ more occurrences when the two criteria are met as a function of the delay time, which could explain why the bleaching oscillations are more pronounced in the case of $C_2D_4^+$ than in the case of $C_2H_4^+$.
We analyzed the relaxation paths to the ground state. The relaxation from D1 occurs mainly through the planar conical intersection, the one from D2 involves both the planar and twisted conical intersections and the relaxation from D3 is mainly occurring through the twisted conical intersection. The same was reported for the hydrogenated ethylene cation case except from D2 where it is mainly through the planar conical intersection. The mechanisms of dissociation were also investigated in this thesis. We found out that for initial states on D2 and D3 the D loss and to a certain extent the D_2 loss can occur through several pathways that were not up to now reported in the literature.

The results reported in this study need to be confirmed by running more trajectories for longer times using both SHARC and BOMD. Once this will have been done, we plan to write a joint experimental-theoretical paper with the group of M. Lucchini and M Nisoli.

References

[1] I. N. Levine, *Quantum Chemistry*, 7th edition, Pearson, New York, 2014.

[2] L.González and R.Lindh, editors, 2021, *Quantum Chemistry and Dynamics of Excited States: Methods and Applications.* Wiley, DOI: 10.1002/9781119417774

[3] M.Nisoli, P. Decleva, F. Calegari et al*., Attosecond electron dynamics in molecules*, Chemical Reviews, vol. 117, n° 16, August 2017, p.10760-10825, DOI: 10.1021/acs.chemrev.6b00453

[4] S. Bag, S. Chandra et al., *The attochemistry of chemical bonding*, International Reviews in physical chemistry, vol. 40, n°3, July 2021, p.405-455, DOI: 10.1080/0144235X.2021.1976499

[5] *The Nobel prize in chemistry 1999*, NobelPrize.org, https://www.nobelprize.org/prizes/chemistry/1999/8642-communique-de-presse-le-prix-nobel-de-chimie-de-1999/

[6] P.B Corkum, *Plasma perspective on strong field multiphoton ionization*, Physical Review Letters, vol. 71, n°13, 1993, DOI:10.1103/PhysRevLett.71.1994

[7] *Attoscience for non-specialists* | Research groups | Imperial College London, https://www.imperial.ac.uk/a-z-research/quantum-optics-and-laser-science/research/laser-consortium/current-research/attoscience-for-non-specialists/

[8] M. Lucchini, B. Mignolet et al. *Few-Femtosecond $C_2H_4^+$ Internal Relaxation Dynamics Accessed by Selective Excitation*, The Journal of Physical Chemistry Letters, vol. 13, n°48, December 2022, p. 11169-11175, DOI: 10.1021/acs.jpclett.2c02763.

[9] C. Sannen, G. Raseev, C. Galloy et al., *Unimolecular decay of electronically excited species. II. The $C_2H_4^+$ ion,* The Journal of chemical physics, vol. 74, n°4, February 1981, p 2402-2411, DOI: 10.1063/1.441361.

[10] B.Joalland, T. Mori, et al., *Photochemical dynamics of ethylene cation $C_2H_4^+$,* The Journal of Physical Chemistry Letters, vol. 5, n°8, April 2014, p.1467-1471, DOI: 10.1021/jz500352x

[11] J.C. Lorquet, C. Sannen, G. Raseev, Dissociation of the ethylene cation: mechanism of energy randomization, Journal of the American chemical society, vol. 102, n°27, December 1980, p.7976-7977, DOI: 10.1021/ja00547a045.

[12] F. Costa, Electronic structure study of the reaction $C_2H_4^+ \rightarrow C_2H_2^+ + H_2$, International journal of quantum chemistry, vol. 106, n°13, 2006, p.2763-2771, DOI: 10.1002/qua.21093

[13] G. Pandey, S. Ghosh, A. K. Tiwari, *Dissociative ionization of the H2 molecule under a strong elliptically polarized laser field: carrier-envelope phase and orientation effect*, Physical Chemistry Chemical Physics, vol. 24, n°39, 2022, p. 24582-24592, DOI: 10.1039/d2cp02292c

[14] M. Lucchini, et al., *Time-resolved ultrafast relaxation dynamics in ethylene cation, private communication unpublished*, March 2019

[15] *Chemistry*, Wikipédia, https://en.wikipedia.org/wiki/Chemistry

[16] N.Poirier, *Born-Oppenheimer Molecular Dynamics using the Variational Quantum Eigensolver*, master thesis, Department of Mechanical Engineering McGill University Montreal, QC, December 2019

[17] S.Matsika and P. Krause, *Nonadiabatic events and conical intersections*, Annual Review of physical Chemistry, vol. 62, p. 621 – 643, DOI : 10.1146/annurev-physchem-032210-103450.

[18] W. Domcke and D. R. Yarkony, *Role of conical intersections in molecular spectroscopy and photoinduced chemical dynamics*, Annual Review of physical chemistry, vol. 63, n°1, May 2012, p. 325-352, DOI : 10.1146/annurev-physchem-032210-103522

[19] S. Mai, P. Marquetand, L.González, *Nonadiabtic Dynamics : the SHARC approah*, WIREs Computational Molecular Science, vol. 8, n°6, November 2018, DOI : 10.1002/wcms.1370

[20] Q-CHEM, User Manual, Section 8*, Basis set and effective core potentials*, https://manual.q-chem.com/latest/Ch8.S1.SS1.html

[21] M. Lucchini, B. Mignolet et al. *Few-Femtosecond $C_2H_4^+$ Internal Relaxation Dynamics Accessed by Selective Excitation*, The Journal of Physical Chemistry Letters, vol. 13, n°48, December 2022, p. 11169-11175, Supporting Information, DOI: 10.1021/acs.jpclett.2c02763

[22] B.Mignolet, *Ethylene dynamics*, [PowerPoint Presentation], 2019

[23] *L'effet isotopique cinétique*, CultureSciences-Chimie, https://culturesciences.chimie.ens.fr/thematiques/chimie-organique/synthese-et-retrosynthese/l-effet-isotopique-cinetique

[24] Etude des effets isotopiques en chimie organique, http://perso.numericable.fr/chimorga/Niveau_M2/isotop/isotop.php

[25] SHARC3.0 | Surface Hopping including Arbitrary Couplings created by the González Group, https://sharc-md.org

[26] BOMD | Gaussian.com, https://gaussian.com/bomd/

[27] S. Mai, D. Avagliano, M. Heindl, P. Marquetand, M.F.S.J. Menger, M. Oppel, F. Plasser, S. Polonius, M. Ruckenbauer, Y. Shu, D.G. Truhlar, L. Zhang, P. Zobel, L. González *SHARC3.0: Surface Hopping Including Arbitrary Couplings – Program Package for Non-Adiabatic Dynamics*,https://sharc-md.org/ (2023). DOI: 10.5281/zenodo.7828641

[28] Manual | SHARC3.0., https://sharc-md.org/?page_id=50#tth_sEc3.2

[29] S-C.Chen, M-C Liu et al., *Photodissociation and infrared spectra of ethylene cations in solid argon*, Chemical Physics Letters, vol. 630, June 2015, p.96-100, DOI: 10.1016/j.cplett.2015.04.050

[30] S.Willitsch, U.Hollenstein, F.Merkt, *Ionization from a Double Bond: Rovibronic Photoionization Dynamics of Ethylene, Large Amplitude Torsional Motion and Vibronic Coupling in the Ground State of* $C_2H_4^+$. J. Chem. Phys. 2004, 120, 1761−1774.